



# Low-Temperature Clay Mineral Dehydration Contributes to Porewater Dilution in Bering Sea Slope Subseafloor

Akira Ijiri<sup>1,2\*</sup>, Naotaka Tomioka<sup>1</sup>, Shigeyuki Wakaki<sup>1</sup>, Harue Masuda<sup>3</sup>,  
Katsumi Shozugawa<sup>4</sup>, Sunghan Kim<sup>5</sup>, Boo-Keun Khim<sup>6</sup>, Masafumi Murayama<sup>7</sup>,  
Motoyuki Matsuo<sup>4</sup> and Fumio Inagaki<sup>1,2,8</sup>

<sup>1</sup> Kochi Institute for Core Sample Research, Japan Agency for Marine-Earth Science and Technology, Nankoku, Japan, <sup>2</sup> Research and Development Center for Submarine Resources, Japan Agency for Marine-Earth Science and Technology, Yokosuka, Japan, <sup>3</sup> Department of Biology and Geosciences, Osaka City University, Osaka, Japan, <sup>4</sup> Graduate School of Arts and Sciences, University of Tokyo, Tokyo, Japan, <sup>5</sup> Division of Polar Paleoenvironment, Korea Polar Research Institute, Incheon, South Korea, <sup>6</sup> Department of Oceanography, Pusan National University, Busan, South Korea, <sup>7</sup> Center for Advanced Marine Core Research, Kochi University, Nankoku, Japan, <sup>8</sup> Research and Development Center for Ocean Drilling Science, Japan Agency for Marine-Earth Science and Technology, Yokohama, Japan

## OPEN ACCESS

### Edited by:

Timothy Ferdman,  
Max Planck Institute for Marine  
Microbiology (MPG), Germany

### Reviewed by:

Christian März,  
University of Leeds, United Kingdom  
Ilya Bindeman,  
University of Oregon, United States

### \*Correspondence:

Akira Ijiri  
ijiri@jamstec.go.jp

### Specialty section:

This article was submitted to  
Biogeoscience,  
a section of the journal  
Frontiers in Earth Science

**Received:** 12 January 2018

**Accepted:** 03 April 2018

**Published:** 19 April 2018

### Citation:

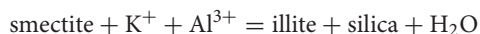
Ijiri A, Tomioka N, Wakaki S,  
Masuda H, Shozugawa K, Kim S,  
Khim B-K, Murayama M, Matsuo M  
and Inagaki F (2018)  
Low-Temperature Clay Mineral  
Dehydration Contributes to Porewater  
Dilution in Bering Sea Slope  
Subseafloor. *Front. Earth Sci.* 6:36.  
doi: 10.3389/feart.2018.00036

Widespread diagenesis of clay minerals occurs in deeply buried marine sediments under high-temperature and high-pressure conditions. For example, the smectite-to-illite (S-I) transformation has been often observed in sediments at *in situ* temperatures above ~60°C. However, it remains largely unknown whether such diagenetic processes naturally occur in relatively shallow and low-temperature sediments and, if so, what the consequences are of any related chemical reactions to the geochemical characteristics in the deep biosphere. We evaluated the possibility of naturally occurring S-I transformation at temperatures below 40°C in continental slope sediments of the Bering Sea by examining porewater chemistry, clay mineralogy, and chemical composition of clay minerals measured to ~800 m beneath the seafloor (mbsf) in core samples acquired during Integrated Ocean Drilling Program Expedition 323. In porewater from these cores, chloride concentrations decreased with increasing depth from 560 mM near the seafloor to 500 mM at ~800 mbsf;  $\delta^{18}\text{O}$  increased from 0 to 1.5‰; and  $\delta\text{D}$  decreased from -1 to -9‰. These trends are consistent with the addition of water derived from S-I transformation. The discrete low  $\text{Cl}^-$  spikes observed between ~200 and ~450 mbsf could be attributed to the dissociation of methane hydrate. X-ray diffraction analysis of the clay-size fraction (<2  $\mu\text{m}$ ) showed an increase of illite content in the I/S mixed layer with increasing depth to 150 mbsf. This increase may imply the occurrence of S-I transformation. The decrease of  $\text{Fe}^{3+}/\text{Fe}^{2+}$  in the clay-size fraction with increasing depth strongly suggests microbial reduction of Fe(III) in clay minerals with burial, which also has the potential to promote the S-I transformation. Our results imply the significant ecological roles on the diagenesis of siliciclastic clay minerals underlying the high-productivity surface seawater at continental margins.

**Keywords:** smectite-to-illite transformation, porewater chemistry, clay mineralogy, iron reduction, Bering Sea Slope

## INTRODUCTION

The smectite-to-illite (S-I) transformation is a ubiquitous and important feature of post-sedimentary alteration processes. Smectite is primarily formed by alteration of volcanoclastic materials (Banfield et al., 1991). During burial diagenesis, smectite is transformed to the more stable clay mineral illite. This process releases silica, interlayer water, and cations associated with K fixation (e.g., Perry and Hower, 1972; Freed and Peacor, 1989; Huang et al., 1993), as indicated in the following reaction (Perry and Hower, 1972):



The release of silica and cations has been suggested as a source of silica or carbonate cements, affecting the porosity of associated sediment (e.g., Hower et al., 1976; Lynch et al., 1997). The release of water may induce high pore-fluid pressure, faulting, and migration of hydrocarbon gases (Bruce, 1984; Freed and Peacor, 1989; Brown et al., 2001). The S-I transformation is conventionally considered to be promoted at high temperature and high pressure conditions in deep burial sediments (Perry and Hower, 1970; Eberl and Hower, 1976; Hower et al., 1976; Freed and Peacor, 1989; Pytte and Reynolds, 1989). The optimal temperature range for this reaction is ca. 60–160°C. Therefore, the transformation proceeding through illite-smectite (I/S) mixed-layer intermediates, in which the percentage of illite layers increases with increasing temperature, has been used as a geothermometer to constrain estimates of a basin's history (e.g., Perry and Hower, 1970; Pytte and Reynolds, 1989; Huang et al., 1993). However, the S-I transformation is more complex than conventional thought and that chemical variables may also affect the rate of reaction (e.g., Inoue et al., 1988; Whitney and Northrop, 1988). For example, the transformation is dependent on precursor compositions as on the availability of K<sup>+</sup> and Al<sup>3+</sup> from other mineral phases (Kastner et al., 1991). The rate of transformation is also affected by the abundance of water in the system (Whitney, 1990). Reducing the water content retards the S-I transformation.

In addition to the physically and chemically driven clay mineral alteration, experimental studies have demonstrated that microbial reduction of Fe(III) in smectite promotes S-I transformation at temperatures below 40°C (Kim et al., 2004; Koo et al., 2016). Kim et al. (2004) inferred that this process occurs through a decrease of the positive charge in the octahedral sheet as a result of Fe(III) reduction accompanied by K fixation in the interlayers to balance the charge. Other experimental studies have shown that microbial activity promotes the S-I transformation (Zhang et al., 2007a,b), but the transformation at temperatures below 40°C has rarely been reported in natural sedimentary environments. Buatier et al. (1992) presented evidence based on transmission electron microscope (TEM) observations that some smectite is transformed at temperatures below 30°C associated with the décollement zone in the Barbados accretionary wedge, where the water/rock ratio is high and fluid circulation is very active. However, direct evidence is lacking

for microbial promotion of S-I transformation in the natural environment.

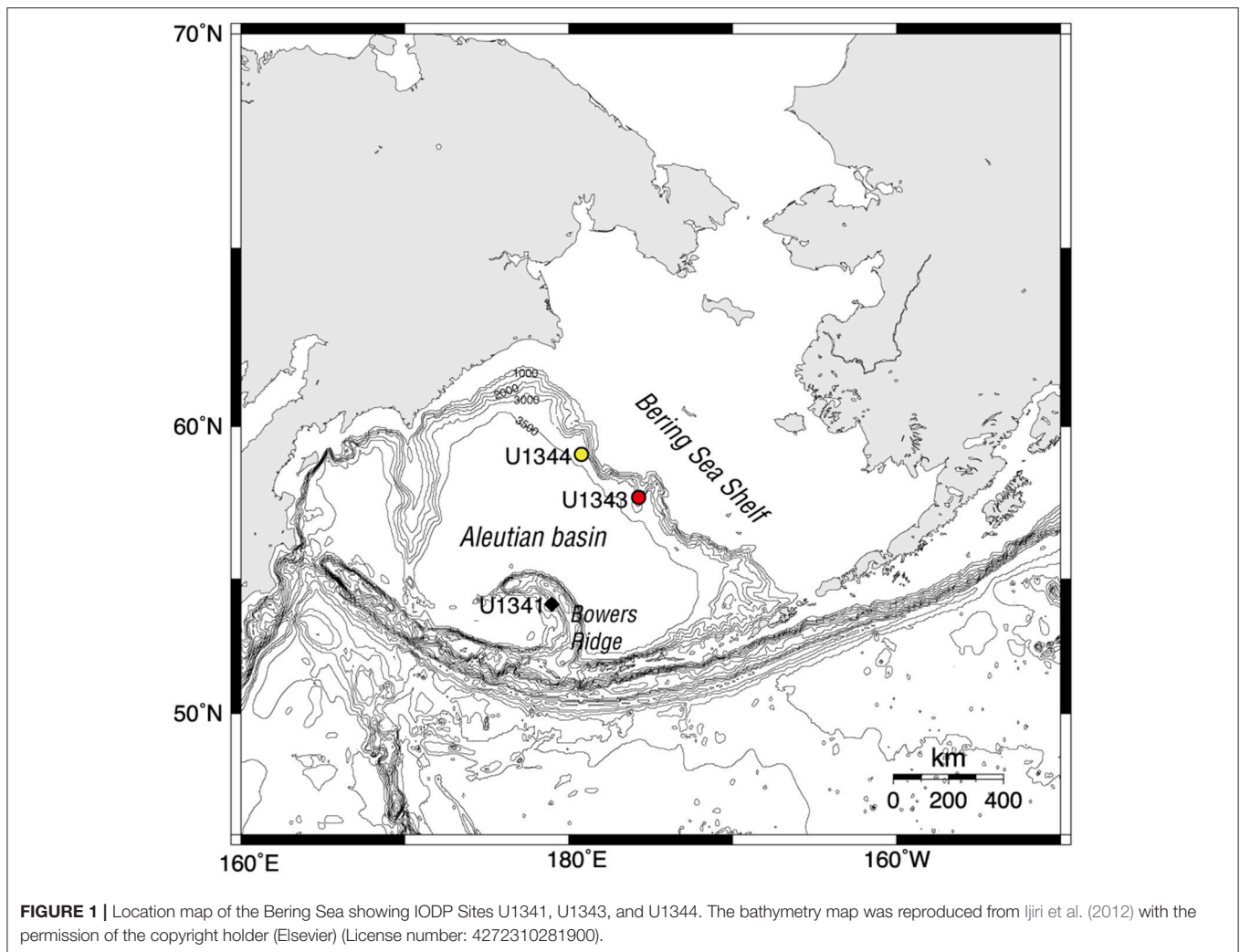
In this context, it has been presumed that clay mineral dehydration has been promoted by microbial Fe(III) reduction in Bering Sea Slope sediments on the basis of porewater chemistry obtained during Integrated Ocean Drilling Program (IODP) Expedition 323 (Takahashi et al., 2011a; Pierre et al., 2016). In Bering Sea Slope sediments, the significant decreases of both porewater salinities and Cl<sup>-</sup> concentrations between ~150 and 300 mbsf have been attributed to the release of low-salinity crystal water from S-I transformation (Takahashi et al., 2011b). In addition, Fe-rich authigenic carbonates formed during later diagenesis and deeper burial from a <sup>13</sup>C-enriched dissolved inorganic carbon pool related to methanogenesis have been observed (Pierre et al., 2016). The precipitation of Fe-rich carbonate requires not only dissolved inorganic carbon but also dissolved Fe<sup>2+</sup> in porewater. Indeed, elevated dissolved Fe<sup>2+</sup> concentrations in porewater with a concentration peak of around 100 mbsf have been observed (Takahashi et al., 2011b). Based on these observations, Pierre et al. (2016) hypothesized that the reduction of Fe(III) in clay minerals by methanogen promotes low-temperature S-I transformation and subsequently releases Fe<sup>2+</sup> to porewater. However, the onboard porewater chemistry results are not evidence for either the release of crystal water as a result of S-I transformation or the reduction of Fe(III) in clay minerals, because there are other possible explanations for the decrease of salinity, such as the dissociation of methane hydrate (Takahashi et al., 2011b). In addition, supporting mineralogical and chemical data for low-temperature S-I transformation and reduction of Fe(III) in clay minerals are lacking.

In this study, we evaluated the hypothesis that microbial Fe(III) reduction in clay mineral, which can promote S-I transformation, and S-I transformation both occur at temperatures below 40°C in continental slope sediments of the Bering Sea down to ~800 mbsf by examining porewater chemistry, clay mineralogy, and chemical compositions of clay minerals.

## ENVIRONMENTAL SETTING

The Bering Sea is a marginal sea of the North Pacific Ocean that is enclosed by the Alaska Peninsula to the east and northeast, the Aleutian Islands to the south, and the Russian mainland and the Kamchatka Peninsula to the west and northwest. Sediment core samples were obtained by the drilling vessel *JOIDES Resolution* at three sites during IODP Expedition 323 in July–September 2009: Site U1343 (water depth 1,952 m, core depth 745 mbsf) and Site U1344 (water depth 3,172 m, core depth 745 mbsf) on the northeastern Bering Sea Slope, and Site U1341 (water depth 2,177 m, core depth 600 mbsf) on Bowers Ridge, which extends ~300 km northward from the Aleutian Islands (**Figure 1**).

The Bering Sea Slope is an area of extremely high primary production, where nutrients are probably transported from the euphotic zone by tidal mixing on the continental shelf and slope as well as by transverse circulation in the Bering Slope Current, including mesoscale eddies near the shelf edge (e.g.,



Springer et al., 1996). Siliciclastic material is the dominant component of the Bering Sea Slope sediments. The sedimentation rate is very high because the input of siliciclastic material from the continental shelf is large (21–58 cm  $\text{ky}^{-1}$  at Site U1343 and 29–50 cm  $\text{ky}^{-1}$  at Site U1344; see Takahashi et al., 2011a), and the burial rate of organic carbon is also high, providing favorable sedimentary habitats for organic-fueled microbial communities (Wehrmann et al., 2011; Kallmeyer et al., 2012). The geothermal gradients measured at depths down to 130–140 mbsf at Sites U1343 and U1344 are 49.0 and 53.3°C  $\text{km}^{-1}$ , respectively (Takahashi et al., 2011b). If it can be assumed that these gradients are linear throughout the cored sediment columns, then the *in situ* temperatures in the cores should be generally below 40°C.

Site U1341, at Bowers Ridge, is in the open marine domain of the Bering Sea (Takahashi et al., 2011a). The sediments there are dominated by diatomic oozes and the sedimentation rate is  $\sim 12$  cm  $\text{ky}^{-1}$  (Takahashi et al., 2011a). The geothermal gradient at Bowers Ridge, at 67.8°C  $\text{km}^{-1}$ , is steeper than the gradient at the Bering Sea Slope sites. Given the high thermal gradient at Site 1341, the depth where S-I transformation occurs is the shallowest as Site 1341.

## MATERIALS AND METHODS

### Analyses of Porewater Samples

Porewater samples were extracted on board after core recovery by using a stainless steel squeezer (Manheim and Sayles, 1974; Takahashi et al., 2011b). Concentrations of  $\text{Cl}^-$  and  $\text{K}^+$  in the porewater samples were measured on board with an ion chromatograph, and dissolved Fe concentration was also measured on board by inductively coupled plasma optical emission spectroscopy (Takahashi et al., 2011b).

Oxygen isotopic compositions ( $\delta^{18}\text{O}$ ) of porewater samples were analyzed at the Kochi Core Center (KCC) by using a mass spectrometer (GV IsoPrime, UK) with an automated  $\text{CO}_2$ - $\text{H}_2\text{O}$  equilibration system (GV MultiPrep, UK). The standard deviation from repeated oxygen isotope analyses of the laboratory standard (Indian Ocean deep sea water) was  $<0.03\text{‰}$ . Results are presented here as per mil deviation from Vienna Standard Mean Ocean Water (VSMOW).

Hydrogen isotopic compositions ( $\delta\text{D}$ ) of porewater samples were analyzed by laser absorption spectroscopy (LWIA-24-EP, Los Gatos Research Inc., USA) at KCC. The standard deviation

from repeated hydrogen isotope analysis of the laboratory standard (Indian Ocean deep seawater) was  $<0.3\%$ .

## Sediment Samples

Sediment aliquot samples for analyses of the mineral and chemical compositions of the clay-size fraction were collected at the KCC from core samples taken at Sites U1341, U1343, and U1344. The sampling interval was 50 m at depths shallower than 300 mbsf and 100 m at depths below 300 mbsf. The sediment comprises mainly two components, opaline diatom valves, and siliciclastic grains (mainly clay and fine silt size) (Aiello and Ravelo, 2012). The sediment from Site U1341 on the Bowers Ridge is mainly composed of the biogenic sediment. The terrigenous sources are a Kamchatkan-Aleutian and the Yukon River (Aiello and Ravelo, 2012). The Aleutian Ridge, a volcanic-plutonic arc, is the source for the majority of the abundant pyroclastic material.

The clay-size fraction ( $<2\ \mu\text{m}$ ) was separated by centrifuge at 1,500 rpm for 1 min. The size of the clay-size fraction in the bulk sediment was determined by weighing the dried bulk sediment sample and the separated clay-size fraction.

## X-Ray Diffraction Analysis of the Clay-Size Fraction

We performed X-ray diffraction (XRD) analysis to determine the mineralogy of the clay-size fractions. Suspensions of clay were dropped onto glass slides and dried in an oven at  $50^\circ\text{C}$  to prepare oriented samples. XRD patterns of oriented samples were obtained with an X-ray diffractometer (Spectris PANalytical, X'pert PRO MPD) using  $\text{CuK}\alpha$  radiation at 40 kV and 40 mA, with  $1/2^\circ$  divergence and anti-scattering slits, a  $1/2^\circ$  receiving slit, and a  $0.021^\circ\ \text{s}^{-1}$  scan rate at steps of  $0.017^\circ$  in  $2\theta$ . After this scanning, the samples were saturated with ethylene glycol (EG) vapor at  $50^\circ\text{C}$  for more than 5 h (referred to here as the EG state), and then the XRD scanning was repeated. For each sample, the saturation in EG vapor and XRD scanning were performed twice, that is, the same oriented sample was saturated with EG vapor again for 5 h and rescanned.

We calculated the proportions of illite and smectite crystallites in the illite/smectite (I/S) mixed-layer phases by employing the technique of Moore and Reynolds (1997), using the angular separation ( $\Delta 2\theta$ ) between the composite illite-(001)/smectite-(002) reflection (at  $2\theta \approx 10.5^\circ$ ) and the composite illite-(002)/smectite-(003) reflection (at  $2\theta \approx 16^\circ$ ) to determine the I/S ratio. For the objective determination of the angle of the subtle peaks of the composite illite-(001)/smectite-(002) reflection and the composite illite-(002)/smectite-(003) reflection, we used the software package X'Pert HighScore (PANalytical B.V., Netherlands). First, we subtracted the baseline from the XRD spectrum, and then the angles of the peaks were automatically determined by the software. We used the average values for the angles determined from duplicate XRD scanning. The average errors in the interlayer smectite percentage when this method is used have been reported to be 2–8% (Hathon, 1992). We also used previously published XRD data for sample splits from Site U1343 (Kim et al., 2015) to calculate the illite content in the I/S mixed-layer phase. In total, we used data from 184 splits of sediment

samples from Site U1343. These splits were retrieved at intervals of  $\sim 1.6\ \text{m}$  at 0–145 mbsf and  $\sim 5\ \text{m}$  at 330–745 mbsf. We used an age model for Site U1343 based on oxygen isotope stratigraphy of benthic foraminifers for the same site (Asahi et al., 2014; Kim et al., 2015) to classify the XRD data from Site U1343 into glacial or interglacial sediments.

The proportions of dominant clay minerals in the clay-size fraction were estimated semi-quantitatively following Biscaye (1965). We identified the small contribution of kaolinite(002) in the peak at  $24\text{--}26^\circ$  and decomposed this peak into elementary peaks of kaolinite(002) and chlorite(004) using Profile Fit Software (Philips PROFIT v.1.0) (Guo and Underwood, 2011). We then determined the relative compositions of kaolinite and chlorite.

## Transmission Electron Microscope Observations

Two sediment samples in which high peak intensities of clay minerals were observed in the X-ray diffractograms for the Site U1343 core were subjected to TEM analysis: 28H-5w-70-71cm (267.7 mbsf) and 83X-6w-75-76cm (778.175 mbsf). The samples were embedded in LR White epoxy resin (hard grade) as described by Kim et al. (1995) and Uramoto et al. (2014). A previous problem in TEM investigation of I/S mixed-layer minerals was the collapse of expandable interlayers under high vacuum, making the discrimination of smectite and illite layers very difficult. Recent improvements in imaging and sample preparation techniques have addressed this problem by the permanent expansion of smectite interlayers using L.R. White resin (Kim et al., 1995). A portion was processed into an ultrathin foil measuring  $10 \times 5\ \mu\text{m}$  and  $\sim 100\ \text{nm}$  thick, using a Ga-ion beam after deposition of carbon protection layers in a focused ion beam apparatus (FIB, Hitachi SMI4050). The foil was mounted on a Cu grid and then studied using a TEM (JEOL JEM-ARM200F) operated at an accelerating voltage of 200 kV. Microtextures were investigated by the lattice fringe imaging technique. Chemical compositions of the mineral particles were obtained by an energy-dispersive X-ray spectrometer with a 100  $\text{mm}^2$  silicon drift detector, using a beam spot size larger than 20 nm and an acquisition time shorter than 30 s to minimize selective elemental loss due to electron beam damage during measurement.

## $^{57}\text{Fe}$ Mössbauer Spectroscopy of the Clay-Size Fraction

To identify the chemical states of iron in the clay-size fractions, we investigated 12 samples from Site U1343 and 6 samples from U1344 by  $^{57}\text{Fe}$  Mössbauer spectroscopy. Mössbauer spectra were measured with a Topologic Systems MFD-110D Mössbauer spectrometer at the University of Tokyo by using a 1.11 GBq  $^{57}\text{Co}/\text{Rh}$  source at room temperature. By comparing the Mössbauer parameters (isomer shift, quadrupole splitting, and internal magnetic field) to standard data, we identified  $\text{Fe}^{2+}$  and  $\text{Fe}^{3+}$  constituents and then calculated their relative abundances. Mössbauer spectra were calculated by a least-squares method

with restrictions of intensity and half-width of peaks. All doublets were treated as symmetric.

## Major and Trace Elements of the Clay-Size Fraction

The major-element concentrations of the clay-size fractions were analyzed by inductively coupled plasma mass spectrometry (ICP-MS). The clay-size fractions were decomposed by mixed HF-HNO<sub>3</sub> acids, dried, and dissolved in 3 M HNO<sub>3</sub>. Samples were diluted and measured with the Agilent 7700 ICP-MS at the KCC using In as an internal standard.

## RESULTS

### Porewater Chemistry

At both sites on the Bering Sea Slope (U1343 and U1344), the Cl<sup>-</sup> concentrations in porewater generally decreased with increasing depth from ~560 to 500 mM, although the values varied widely (Figures 2A,B). At Site U1343, the concentrations at depths shallower than 420 mbsf were scattered, and some negative excursions (discrete low Cl<sup>-</sup> spikes) were observed between 150 and 420 mbsf (Figure 2A). At Site U1344, concentrations were also scattered, with discrete low Cl<sup>-</sup> spikes around 270 and 360 mbsf (Figure 2B). At Site U1341 on Bowers Ridge, the Cl<sup>-</sup> concentration was nearly constant at ~550 mM (Figure 2C).

The K<sup>+</sup> concentration in porewater at Site U1343 slightly increased from 10 mM near the sediment surface to 12 mM at 150 mbsf, then decreased to ~6 mM at greater depths (Figure 2D). The K<sup>+</sup> concentration decreased with increasing depth at Site U1344, (Figure 2E), but no decrease was observed at Site U1341 (Figure 2F).

The dissolved Fe concentrations in porewater at Sites U1343 and U1344 were highly scattered, ranging from 0 to 80 μM (Figures 2G,H). At Site U1343, the Fe concentration reached a maximum of 60 μM at ~50 mbsf and was <25 μM below a depth of 100 mbsf (Figure 2G). At Site U1344, the Fe concentration reached a maximum of 80 μM at 100–200 mbsf and was <30 μM below 400 mbsf (Figure 2H). At Site U1341, the Fe concentration reached a maximum value of 17 μM at 4 mbsf and was <5 μM or not detected below 20 mbsf (Figure 2I).

The vertical profiles of δ<sup>18</sup>O and δD in porewater at all three sites showed peaks at around 30–50 mbsf (Figures 3A–F). At Site U1343, δ<sup>18</sup>O increased from +0.2 to +1.8‰ with increasing depth, whereas δD continued to decrease from -2 to -10‰ with increasing depth below ~120 mbsf (Figures 3A,D). At Site U1344, δ<sup>18</sup>O increased from +0.2 to +1.4‰, whereas δD continued to decrease from -2 to -9‰ with increasing depth below ~140 mbsf (Figures 3B,E). At Sites U1343 and U1344, the δ<sup>18</sup>O and δD-values below 120–140 mbsf were strongly negatively correlated (Figures 3G,H). Their changes seemed to be proportional to the decrease in Cl<sup>-</sup> concentrations (Figures 2A,B) with increasing depth. More specifically, the plots of Cl<sup>-</sup> concentrations vs. δ<sup>18</sup>O and δD below 120–140 mbsf at Sites U1343 and U1344 show two trends.

The discrete low Cl<sup>-</sup> spikes observed between ~200 and ~450 mbsf at Sites U1343 and U1344 show <sup>18</sup>O enrichment proportional to Cl<sup>-</sup> depletion with weak to moderate correlation, but very weak or no correlation between Cl<sup>-</sup> and δD ( $R^2 < 0.1$ )

(Figures 4A,B,D,E). At Site U1343, the discrete low Cl<sup>-</sup> spikes observed between 141 mbsf and 225 mbsf show no relationship with δ<sup>18</sup>O and δD, but the discrete low Cl<sup>-</sup> spikes between 247 and 423 mbsf show a weak correlation in that the enrichment of <sup>18</sup>O is proportional to the depletion of Cl<sup>-</sup> ( $R^2 = 0.31$ ) (Figures 4A,D). At Site U1344, the discrete low Cl<sup>-</sup> spikes at around 270 and 360 mbsf show that enrichment of <sup>18</sup>O is proportional to the depletion of Cl<sup>-</sup> with a moderate correlation ( $R^2 = 0.55$ ) (Figures 4B,E).

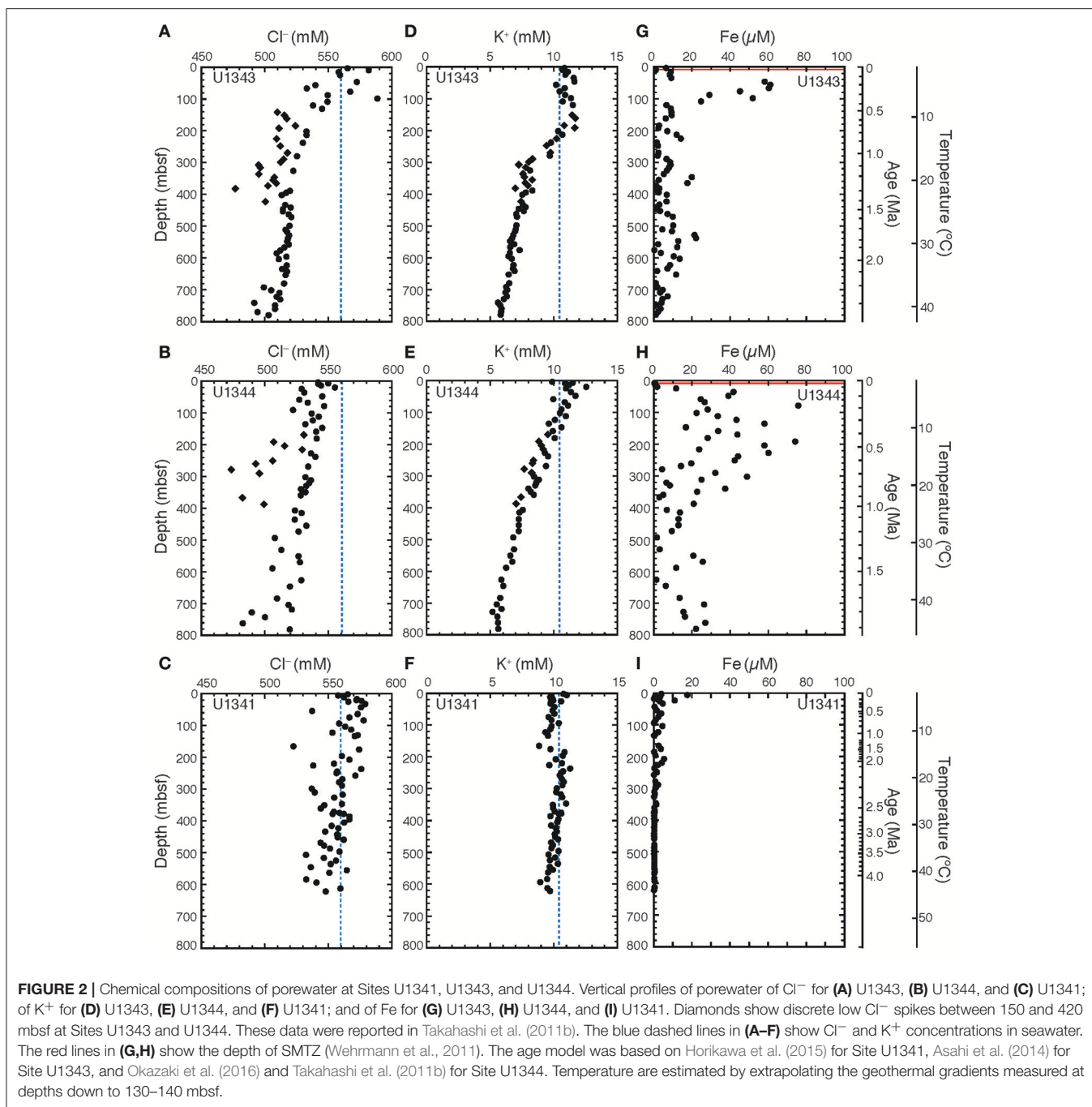
In contrast to the discrete low Cl<sup>-</sup> spikes, most data fall on the trend line that clearly shows <sup>18</sup>O enrichment and D depletion in proportion to Cl<sup>-</sup> depletion. At Site U1343, most porewater data show a moderate correlation between <sup>18</sup>O enrichment and the depletion of Cl<sup>-</sup> ( $R^2 = 0.49$ ) and between D depletion and depletion of Cl<sup>-</sup> ( $R^2 = 0.46$ ) (Figures 4A,D). At Site U1344, most data show a moderate correlation between <sup>18</sup>O enrichment and the depletion of Cl<sup>-</sup> ( $R^2 = 0.58$ ) and a strong correlation between D depletion and depletion of Cl<sup>-</sup> ( $R^2 = 0.65$ ) (Figures 4B,E).

The δ<sup>18</sup>O values at Site U1341 ranged from 0 to +0.6‰. They increased from 0.2‰ at 200 mbsf to 0.6‰ around 270 mbsf, and were almost constant at 0.4‰ below 300 mbsf (Figure 3C). The δD-values from Site U1341 ranged from -0.5 to +3‰. Below the high-δD peak at 60 mbsf, δD-values slightly decreased with increasing depth from 0 to -1‰ (Figure 3F).

### XRD Analysis of the Clay-Size Fraction

Figure 5 shows representative examples of X-ray diffractograms for clay-rich and clay-poor samples taken from Site U1343. The distribution of peaks indicates that the clay-size fraction contained smectite, illite, chlorite, and kaolinite. The peak at  $2\theta \approx 9^\circ$  that was unaffected by EG solvation represents illite (001). The shift of the peak from  $6.4^\circ$   $2\theta$  to  $5.5^\circ$   $2\theta$  by EG saturation indicates a mixture of discrete smectite and mixed-layer I/S. The subtle peak at  $2\theta \approx 10.5^\circ$  represents the composite illite-(001)/smectite-(002) reflection. A composite reflection of illite-(002)/smectite-(003) at  $2\theta \approx 16^\circ$  was detected in the clay-rich sample (Figure 5A; Figures S1, S2). Figure 6 shows vertical profiles of X-ray diffractograms from Sites U1341, U1343, and U1344. The X-ray diffractograms from Sites U1343 and U1344 are similar. The peak intensities of clay minerals were lower in the samples from Site U1341 than in the samples from Sites U1343 and U1344. Composite reflections of illite-(002)/smectite-(003) were detected in the clay-rich samples from the Bering Sea Slope, whereas only a subtle illite-(002)/smectite-(003) peak was observed in the clay-poor Bowers Ridge sample (Figures S1, S2).

The illite content in the I/S mixed layer was estimated from the angular separation ( $\Delta^{\circ}2\theta$ ) between the detected composite reflections of illite-(001)/smectite-(002) and illite-(002)/smectite-(003) (Figure 7; Tables S1, S2). At Site U1343, the inferred illite content in the I/S mixed-layer clay minerals was <6% at depths shallower than 144 mbsf, reached a maximum of 17% at 144 mbsf, and ranged from 5 to 14% with a wide scatter below 144 mbsf. The trend was similar at Site U1344; the content increased from 2% at 40.2 mbsf to 11% at 210.6 mbsf and then decreased to 8% at 485.3 mbsf. At Site U1341, the composite reflections of I/S were detected from only one sample at 164 mbsf, and the estimated illite content was 2% in the I/S mixed layer.



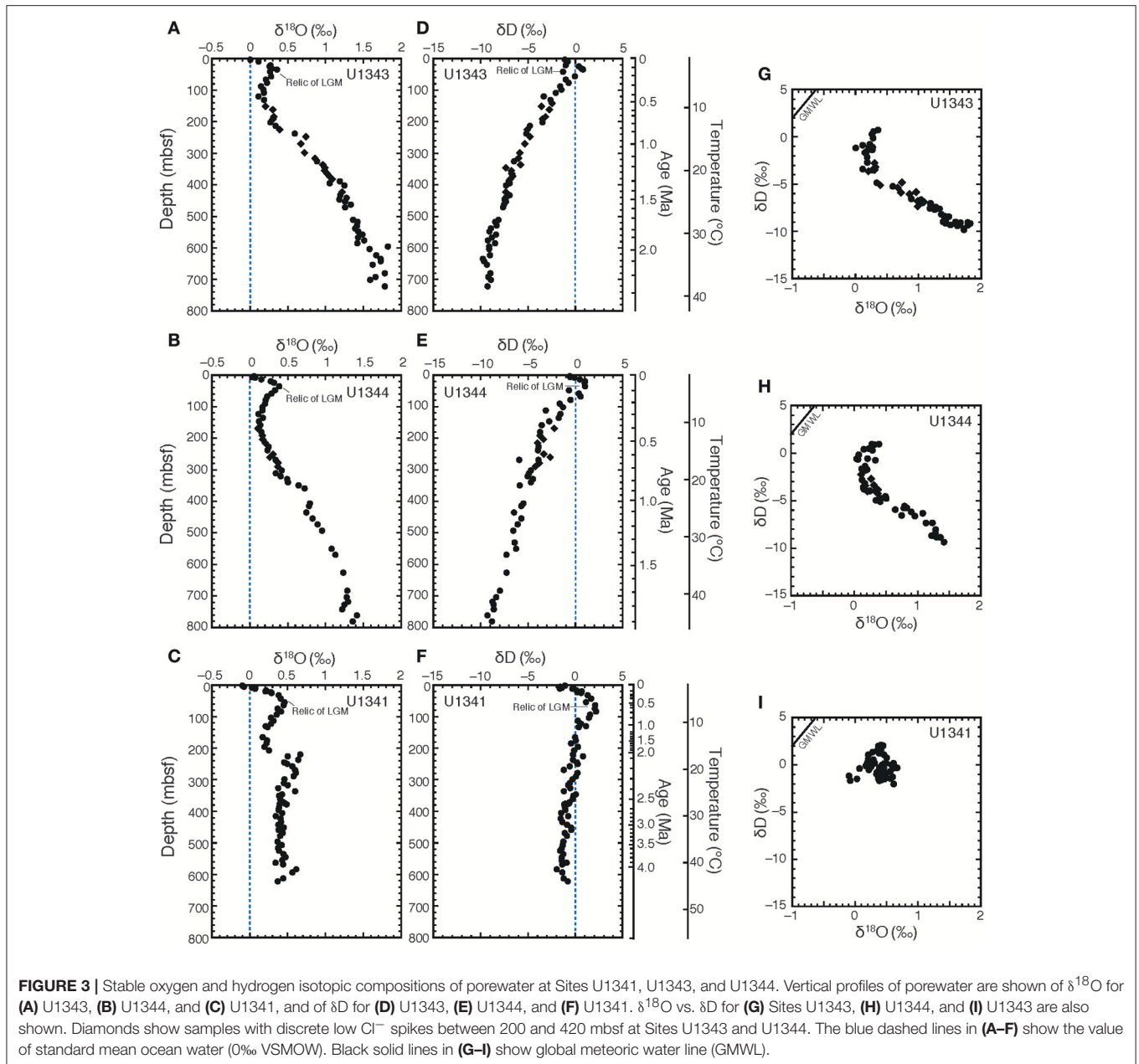
The clay-size fraction made up a larger proportion of each sample at Sites U1343 and U1344 (0.3–24 wt.%, 14 wt.% on average) than it did in the sediments of Site U1341 at Bowers Ridge (0.2–8.3 wt.%, 2.9 wt.% on average) (Figure 8A).

At Sites U1343 and U1344, the contents of smectite, illite, and chlorite + kaolinite in the clay-size fraction were 17–51, 31–53, and 13–33%, respectively (Figure 8B). At Site U1341, some X-ray diffractograms showed very low peak intensities of clay minerals and not all of the compositions could be estimated. The smectite contents were greater and illite contents were smaller than those at Sites U1343 and U1344.

## TEM Observations

We identified particles of smectite, discrete illite, and chlorite in two samples from Site U1343 by TEM observation (Figures S3–S5). We also identified these clay minerals by XRD analysis (Figures 5, 6).

In the upper sample (28H-5w-70-71cm), we found one smectite particle 0.25  $\mu\text{m}$  long containing a small portion of interlayered illite, as shown by a change in layer spacing from 1.3 nm (characteristic of smectite) to 1.0 nm, the (001) interlayer spacing of illite (e.g., Drits et al., 1997) (Figures 9a,b). Energy-dispersive X-ray analysis showed that these layers at the tip of



the smectite particle had higher Al and K contents and lower Mg and Fe contents than the layers in the central part of the same particle, and the Mg/Si, Al/Si, K/Si, and Fe/Si X-ray intensity ratios likewise differed distinctly between the tip and the central part of the particle (Figure 9c).

### $\text{Fe}^{3+}/\text{Fe}^{2+}$ in the Clay-Size Fraction

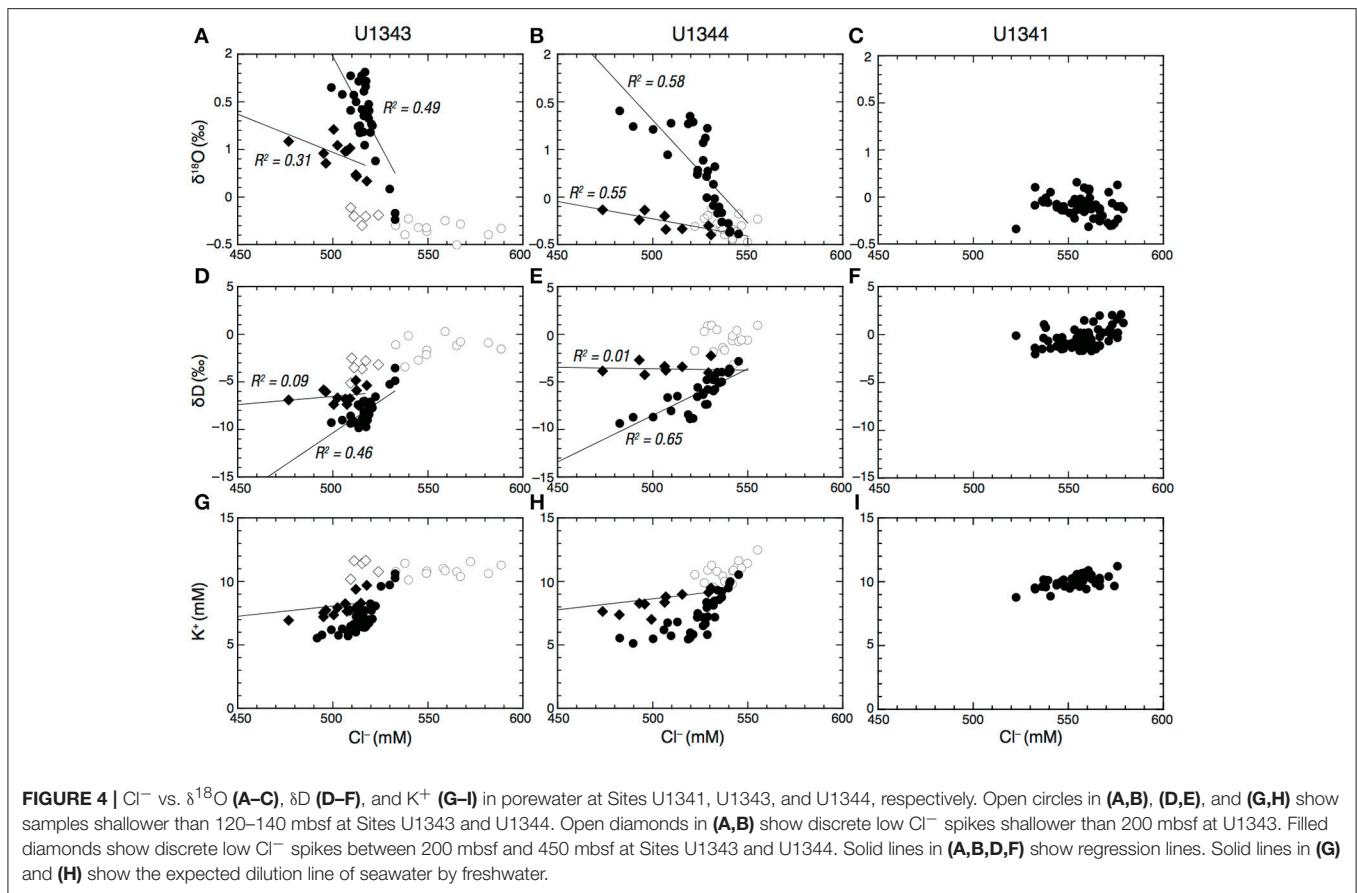
Mössbauer spectroscopy showed that the samples from Sites U1343 and U1344 had similar vertical profiles of  $\text{Fe}^{3+}$  content in total Fe in the clay-size fraction, decreasing from  $\sim 70\%$  near the sediment surface to  $\sim 60\%$  at 300 mbsf and staying at 50–60% below 400 mbsf (Figure 10A). The  $\text{Fe}^{3+}/\text{Fe}^{2+}$  ratios decreased

from  $\sim 2.5$  near the sediment surface to 1.5 at 30 mbsf and were lower than 1.5 below 400 mbsf (Figure 10B).

### Major Elements in the Clay-Size Fraction

The major-element concentrations in the clay-size fraction were similar at Sites U1343 and U1344 (Figure S6, Table S1). The sample from Site U1341 had lower percentages of Mg, Al, K, Ca, and Fe than the samples from Sites U1343 and U1344. The chemical index of alteration (CIA) was calculated by molecular proportion:

$$\text{CIA} = [\text{Al}_2\text{O}_3 / (\text{Al}_2\text{O}_3 + \text{CaO} + \text{Na}_2\text{O} + \text{K}_2\text{O})] \times 100$$



(Nesbitt and Young, 1982) (Figure S7, Table S1). The index at Site U1341 ranged from 18 to 74. The indices at Sites U1343 and U1344 ranged from 61 to 76 (74 on average). The indices at Sites U1343 and U1344 were constant with depth.

## DISCUSSION

### Clay Mineral Dehydration and Dissociation of Methane Hydrates Inferred by Porewater Chemistry

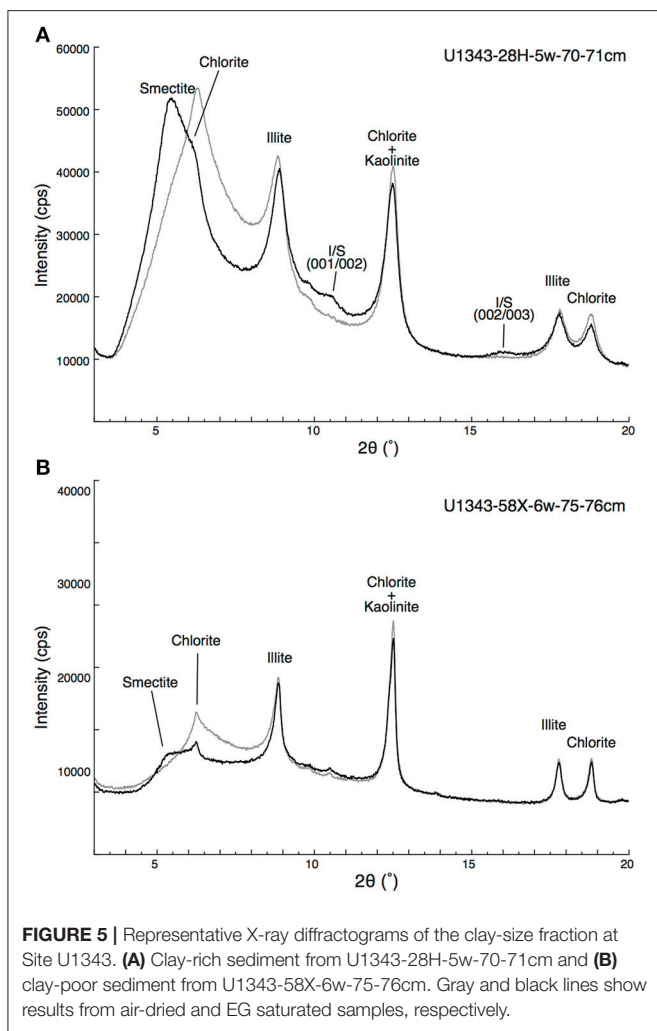
The vertical profiles of porewater chemistry in the Bering Sea Slope (Sites U1343 and U1344) display a decreased  $\text{Cl}^-$  concentration with depth, a trend that was not observed at the Bowers Ridge site (U1341) (Figures 2A–C). The  $\text{Cl}^-$  decrease suggests dilution of the original porewater with freshwater. Possible sources include water released by the dissociation of methane hydrate, freshwater derived from the dehydration of clay minerals (Takahashi et al., 2011b; Pierre et al., 2016), and opal diagenesis (Kastner et al., 1991).

The depletion of  $\text{K}^+$  with depth at Sites U1343 and U1344 may imply  $\text{K}^+$  uptake as interlayer K in newly formed illite during S-I transformation (Perry and Hower, 1972; Takahashi et al., 2011b). However, dilution with freshwater may also cause a decrease in  $\text{K}^+$  concentration. If dilution were the sole cause of the decrease in  $\text{K}^+$  concentration, then both  $\text{K}^+$  and  $\text{Cl}^-$

would decrease in the same proportion. The plots of  $\text{Cl}^-$  vs.  $\text{K}^+$  showed two trends: a decrease in  $\text{K}^+$  concentration consistent with freshwater dilution and a  $\text{K}^+$  concentration that was below the value expected from freshwater dilution (Figures 4G,H). The  $\text{K}^+$  concentrations corresponding to the discrete low  $\text{Cl}^-$  spikes observed between 247 and 423 mbsf at Site U1343, and at around 270 and 360 mbsf at Site U1344 are consistent with freshwater dilution, suggesting that the discrete low  $\text{Cl}^-$  spikes are caused by dilution without  $\text{K}^+$  uptake. In contrast, the other  $\text{K}^+$  concentrations, which are below the value expected from freshwater dilution (Figures 4G,H), suggest that  $\text{K}^+$  was taken up beyond the dilution factor. However, the uptake of  $\text{K}^+$  also occurs in other early diagenetic reactions, such as the exchange of  $\text{K}^+$  for other interlayer cations in smectite and weathered illite (Hover et al., 2002). Consequently, the depletions of  $\text{Cl}^-$  and  $\text{K}^+$  in porewater are not definitive evidence of S-I transformation.

Oxygen and hydrogen isotopic compositions of porewater are important indicators of diagenetic processes and the origin of water. The vertical profiles of  $\delta^{18}\text{O}$  and  $\delta\text{D}$  in porewater at all three sites showed peaks at around 30–50 mbsf (Figures 2A,C). These peaks correspond to the relic of ambient bottom water at the time of the last glacial maximum. The changes in  $\delta^{18}\text{O}$  and  $\delta\text{D}$  of seawater caused by glaciation and deglaciation diffuse down from seafloor, and a large isotopic shift toward low values associated with the last deglaciation was mainly preserved after





the attenuation. As a result, the vertical profile of porewater  $\delta^{18}\text{O}$  and  $\delta\text{D}$  shows an increase over the first 30–50 m below sea floor, followed by a decrease (Schrug and DePaolo, 1993).

There were two trends in the plots of  $\text{Cl}^-$  concentrations vs.  $\delta^{18}\text{O}$  and  $\delta\text{D}$  below 120–140 mbsf at Sites U1343 and U1344. The discrete low  $\text{Cl}^-$  spikes are associated with  $^{18}\text{O}$ -enrichment and no change of  $\delta\text{D}$  in proportion to  $\text{Cl}^-$  depletion, whereas most of the other data show  $^{18}\text{O}$ -enrichment and D depletion in proportion to  $\text{Cl}^-$  depletion (Figures 4A,B,D,E). These two trends strongly suggest that there are two freshwater components for the dilution.

The discrete low  $\text{Cl}^-$  spikes suggest local dilution of the original porewater. The  $\delta^{18}\text{O}$  values of the freshwater component were estimated to be  $+5.0 \pm 4.9\text{‰}$  at Site U1343 and  $+2.1 \pm 1.9\text{‰}$  at Site U1344 (95% confidence interval) by extrapolating  $[\text{Cl}^-] = 0$  to the observed trend with  $^{18}\text{O}$  enrichment in proportion to the  $\text{Cl}^-$  depletion of the discrete low  $\text{Cl}^-$  spikes. These values are 2.5–5‰ higher than those of the base values ( $\delta^{18}\text{O}$ :  $\sim 0\text{‰}$ ) at a  $\text{Cl}^-$  of 530–540 mM. The recrystallization of biogenic opal is a possible source of freshwater in this case because opal diagenesis may enrich  $^{18}\text{O}$  but not affect D in

porewater (Dählmann and De Lange, 2003). Another possible source of freshwater is the dissociation of methane hydrate, if in the sampling process the porewater was diluted by water released from methane hydrate that was enriched in  $^{18}\text{O}$  and D (Hesse and Harrison, 1981). The isotopic fractionation factors of oxygen and hydrogen in water between gas hydrate and liquid water were determined to be 1.0023–1.0032 and 1.014–1.022, respectively (Maekawa, 2004). The estimated end member ( $\text{Cl}^- = 0 \text{ mM}$ )  $\delta^{18}\text{O}$  values of freshwater for the discrete low  $\text{Cl}^-$  spikes, which are 2.2–5‰ higher than the base values ( $\text{Cl}^- \sim 530 \text{ mM}$ ,  $\delta^{18}\text{O} \sim 0\text{‰}$ ), are similar to the previously reported oxygen isotopic fractionation. On the other hand, an unchanging  $\delta\text{D}$  combined with a decreasing  $\text{Cl}^-$  is not consistent with the  $\delta\text{D}$ -value of hydrate water, which is 14–22‰ higher than the surrounding water. However, scattered  $\text{Cl}^-$  values with negative excursions are characteristic of the dissociation of methane hydrate during core recovery and sampling (Ussler and Paull, 2001). Furthermore, regional studies have documented that, in the vicinity of Site U1343, the sequence acoustically displays a vertical series of bottom-simulating reflectors (BSRs). The shallowest reflector, at  $\sim 350 \text{ m}$ , has been linked to the formation of interstitial methane gas hydrate, and a deeper one, at  $\sim 1 \text{ km}$ , has been linked to the diagenetic transition of opal-A to opal-CT (Cooper et al., 1987; Takahashi et al., 2011b). At Site U1344, the posited hydrate BSR is acoustically weak, but the depth of the putative BSR is estimated to be  $\sim 450 \text{ mbsf}$  (Takahashi et al., 2011b). It is therefore possible the discrete low  $\text{Cl}^-$  spikes observed between  $\sim 200 \text{ mbsf}$  and  $\sim 420 \text{ mbsf}$  at Sites U1343 and U1344 can be attributed to the dissociation of methane hydrate during the core recovery. The maximum excursions of the discrete low  $\text{Cl}^-$  spikes from the base values of vertical  $\text{Cl}^-$  profiles are from  $\sim 520$  to 495 mM (4.8%) at around 350 mbsf at Site U1343 (Figure 2A) and from  $\sim 530$  to 473 mM (11%) at 278 mbsf at Site U1344 (Figure 2B), which indicates that the maximum contents of methane hydrate water in the porewater samples are only 4.8 and 11% at Sites U1343 and U1344, respectively. If the isotopic fractionation factor of hydrogen in water between gas hydrate and liquid water is 1.014–1.022 (Maekawa, 2004), then the  $\delta\text{D}$ -values at 350 mbsf at Site U1343 and 278 mbsf at Site U1344 showing the maximum excursion of low  $\text{Cl}^-$  spikes should be 0.6–1.1 and 1.5–2.4‰ higher than the base value of the vertical  $\delta\text{D}$  profiles at Sites U1343 and Site U1344, respectively. These changes would be too small to be separately identified in a large  $\delta\text{D}$  variation.

In contrast to the data associated with the discrete low  $\text{Cl}^-$  spikes, most data plotted on a trend showing  $^{18}\text{O}$  enrichment and D depletion in proportion to  $\text{Cl}^-$  depletion, which clearly indicates that the porewater was originally diluted by a freshwater component other than methane hydrate water. The observed relations between  $\delta^{18}\text{O}$  and  $\delta\text{D}$  at the study sites (Figure 3) are far from the global meteoric water line (Craig, 1961) and make groundwater derived from land (meteoric water) a very unlikely source of the low- $\text{Cl}^-$  fluid. Opal diagenesis is also an unlikely source, because recrystallization of biogenic opal may enrich  $^{18}\text{O}$  but does not affect D in pore water (Dählmann and De Lange, 2003). In addition, shipboard XRD analysis did not reveal any evidence of silica diagenesis including transformation of Opal-A

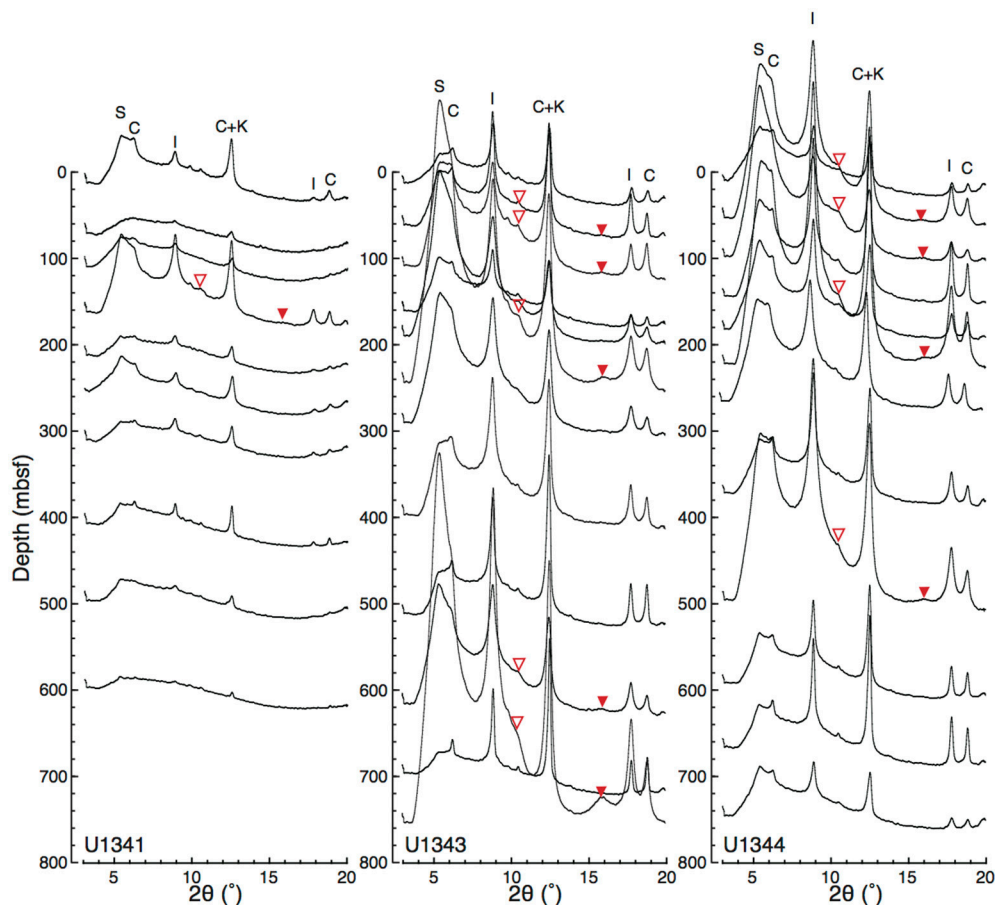


**FIGURE 6** | Vertical profiles of X-ray diffractograms from Sites U1341, U1343, and U1344. The base line of each diffractogram at its left edge ( $2\theta = 3^\circ$ ) corresponds to sampling depth. Open and solid triangles indicate the detected composite reflections of illite-(001)/smectite-(002) and illite-(002)/smectite-(003), respectively. The enlarged views of the detected composite reflections are shown in Figures S1, S2.

to Opal-CT, at Sites U1343 and U1344 (Takahashi et al., 2011b). The enrichment of  $^{18}\text{O}$  and depletion of D in proportion to  $\text{Cl}^-$  depletion at Sites U1343 and U1344 indicate that the most plausible source of the freshwater is the dehydration reaction involving clay minerals, because smectite dewatering during the S-I transformation emits water enriched in  $^{18}\text{O}$  and depleted in D (Kastner et al., 1993; Dählmann and De Lange, 2003). If it is assumed that the isotopic compositions of porewater are determined by simple mixing with freshwater ( $\text{Cl}^- = 0$ ), the  $\delta^{18}\text{O}$  and  $\delta\text{D}$ -values of the freshwater component can be estimated by extrapolating  $[\text{Cl}^-] = 0$  to the observed porewater data; by doing so, the calculated values are  $+20.7 \pm 7.5\text{‰}$  and  $-78 \pm 29\text{‰}$ , respectively, at Site U1343 and  $+12.1 \pm 3.9\text{‰}$  and  $-57 \pm 15\text{‰}$  at Site U1344 (95% confidence interval) (Figures 4, 11). The estimated end member ( $\text{Cl}^- = 0$ )  $\delta^{18}\text{O}$  and  $\delta\text{D}$ -values of the freshwater component at Sites U1343 and U1344 agree fairly well with previously reported stable isotopic compositions of marine clay minerals, which range from +13 to +29‰ for  $\delta^{18}\text{O}$  and from -87 to -30‰ for  $\delta\text{D}$  (Savin and Epstein, 1970; Yeh, 1980; Suchecky and Land, 1983) (Figure 11). The strong negative correlation between  $\delta^{18}\text{O}$  and  $\delta\text{D}$  (Figures 3G-I)

suggests that clay mineral dehydration is a dominant source of the freshwater and dilution by methane hydrate dissociation is a local phenomenon.

Hensen et al. (2004) estimated the temperatures of fluid formation derived from clay mineral dehydration at submarine mud volcanoes, under the assumption the isotopic equilibrium conditions between clay minerals and the surrounding pore water prevail (Sheppard and Gilg, 1996). We calculated the formation temperature of fluid following the method described in Hensen et al. (2004). Under the assumption that the freshwater is derived from clay dehydration and using the estimated end member ( $\text{Cl}^- = 0$ )  $\delta^{18}\text{O}$  and  $\delta\text{D}$ -values of the freshwater as a starting point, we can estimate theoretical  $\delta^{18}\text{O}$  vs.  $\delta\text{D}$ -values for clay minerals to produce the estimated end member  $\delta^{18}\text{O}$  and  $\delta\text{D}$ -values of the freshwater component at different temperatures using previously reported equilibrium fractionation values of  $\delta^{18}\text{O}$  and  $\delta\text{D}$  between clay and water (for  $\delta^{18}\text{O}$ , Sheppard and Gilg, 1996; for  $\delta\text{D}$ , Yeh, 1980; Capuano, 1992) (Figure 11). The previously reported natural  $^{18}\text{O}$  vs. D variability of marine clay can be used to constrain the possible formation temperatures of fluid by comparing them to the

theoretical  $\delta^{18}\text{O}$  vs.  $\delta\text{D}$ -values for clay minerals at different temperatures (Figure 11). In Figure 11, the shaded area shows the previously reported range of  $^{18}\text{O}$  vs. D-values (Savin and

Epstein, 1970; Yeh, 1980; Suchecky and Land, 1983). Where the equilibrium fractionation lines intersect this shaded area, temperatures of 300°C for U1343 and 110°C for U1344 were observed as the lowest values. Because of the large confidence intervals of the estimated end member  $\delta^{18}\text{O}$  and  $\delta\text{D}$ -values for Site U1343, the estimates of formation temperature vary widely between 135°C and infinity. The estimate of the formation temperature for Site U1344 varies from 80 to 180°C. In both cases, the estimated formation temperature is too high for *in situ* formation of the freshwater component in the cored depths, where the temperature is lower than 40°C. We can calculate the formation temperature of fluid by the opposite approach (Figure 12). First, we calculated theoretical  $\delta^{18}\text{O}$  vs.  $\delta\text{D}$ -values for water equilibrated with natural  $^{18}\text{O}$  vs. D of marine clay at different temperatures using previously reported equilibrium fractionation values of  $\delta^{18}\text{O}$  and  $\delta\text{D}$  between clay and water (for  $\delta^{18}\text{O}$ , Sheppard and Gilg, 1996; for  $\delta\text{D}$ , Yeh, 1980; Capuano, 1992). The formation temperature can be estimated by the intersection between the theoretical  $\delta^{18}\text{O}$  vs.  $\delta\text{D}$  of water and the end member  $\delta^{18}\text{O}$  and  $\delta\text{D}$ -values of the freshwater component (Figure 12). The temperatures at the intersections for  $\delta^{18}\text{O}$  are 280°C for U1343 and 110°C for U1344. The temperatures at the intersections for  $\delta\text{D}$  are 170 and 300°C for U1343 and 90°C for U1344.

There are, however, two possibilities for a higher formation temperature. One is that the  $\delta^{18}\text{O}$  and  $\delta\text{D}$  of water derived from clay mineral dehydration is not in equilibrium with those of the clay minerals; the other is that the fluid was derived from several kilometers below the seafloor, where the temperature is >120°C. If it is assumed that the thermal gradients at Sites

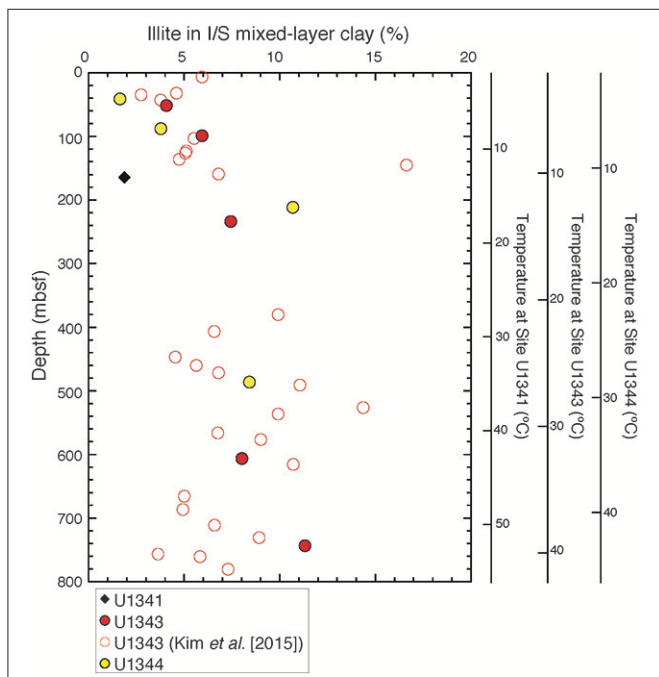


FIGURE 7 | Vertical profile of illite content in the I/S mixed layer at Sites U1341, U1343, and U1344.

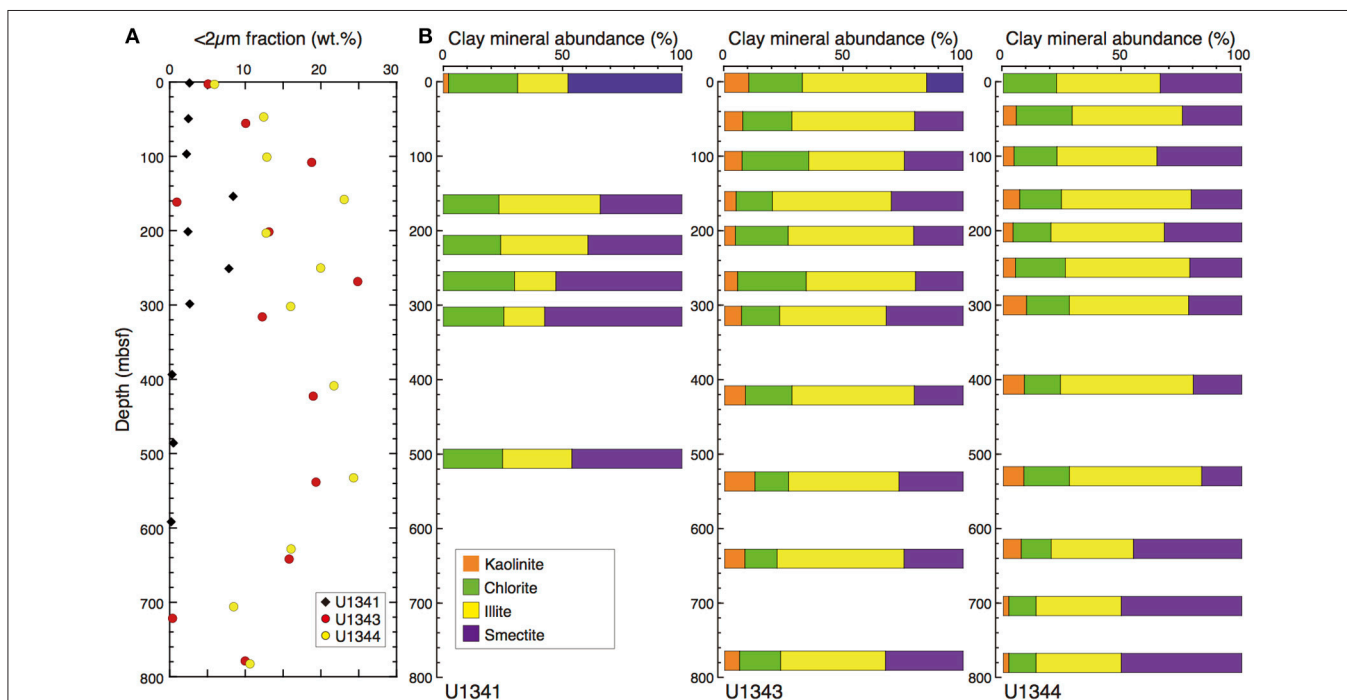
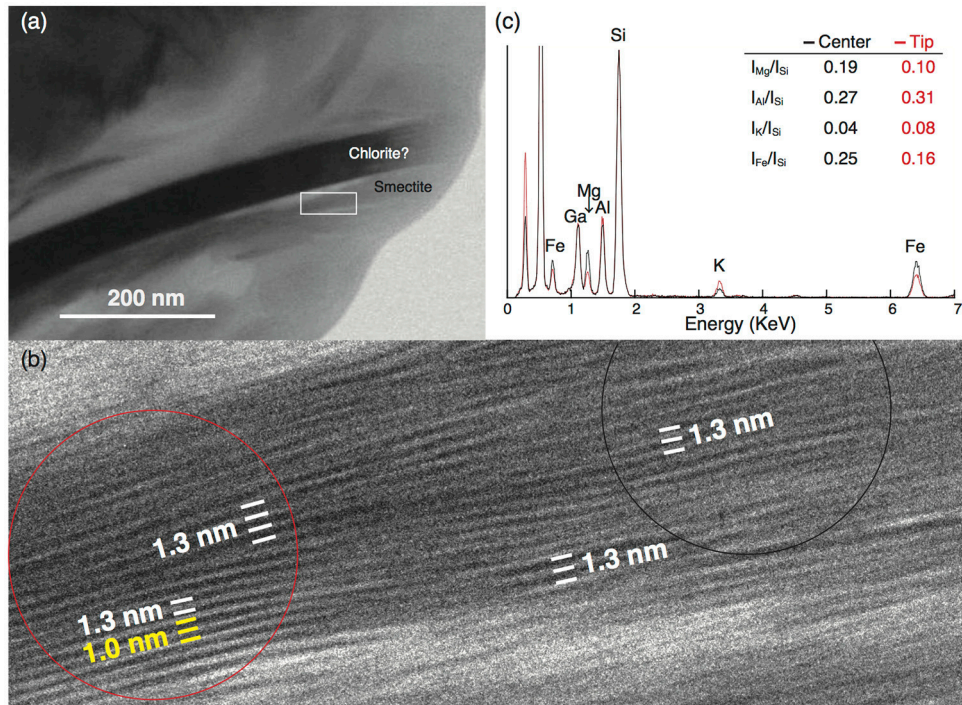
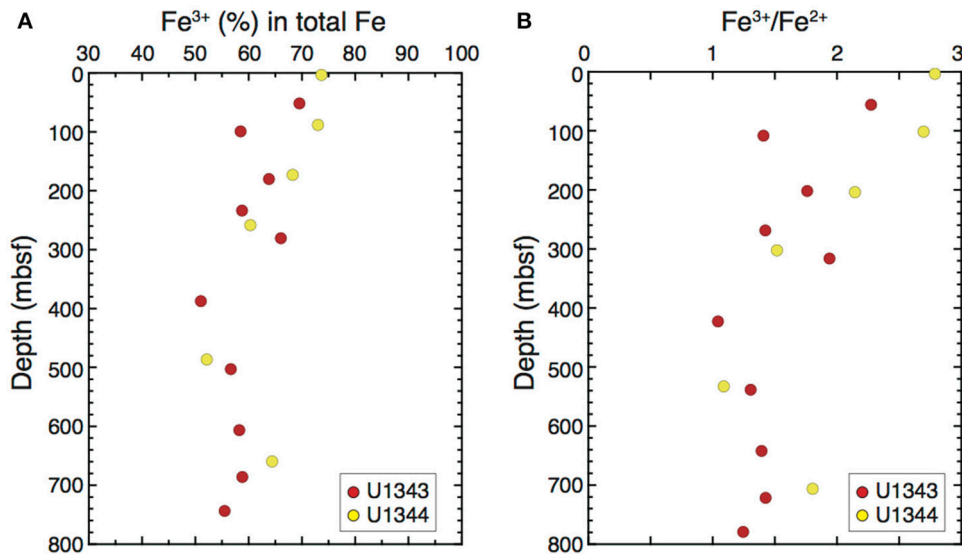


FIGURE 8 | Clay-size fraction (<2 μm) and clay mineral composition at Sites U1341, U1343, and U1344. (A) Vertical profile of the clay-size fraction (<2 μm) in the bulk sediment. (B) Relative percentages of smectite, illite, chlorite, and kaolinite.



**FIGURE 9** | TEM micrograph of a smectite particle in sample 28H-5w-70-71cm (267.7 mbsf) from Site U1343. **(a)** Small smectite particles near a chlorite particle; the white rectangle outlines the area shown in **(b)**. **(b)** High-resolution TEM lattice fringe image showing that smectite (interlayer spacing 1.3 nm) is partly transformed into illite (1.0 nm). Red and black circles outline the areas in the tip and central parts, respectively, that were analyzed by energy-dispersive X-ray spectroscopy (EDS). **(c)** EDS spectra of the tip (red line) and center (black line) of the smectite particle with the ratio of X-ray counts for each element. The intensities of Si peaks were matched to normalize the two spectrums. The Ga peak is an artifact of the Ga-ion beam used during the preparation of the ultrathin foil.



**FIGURE 10** | Vertical profile of the relative abundances of **(A)**  $Fe^{3+}$  in total Fe and **(B)**  $Fe^{3+}/Fe^{2+}$  in the clay-size fraction at Sites U1343 and U1344 determined by  $^{57}Fe$  Mössbauer spectroscopy.

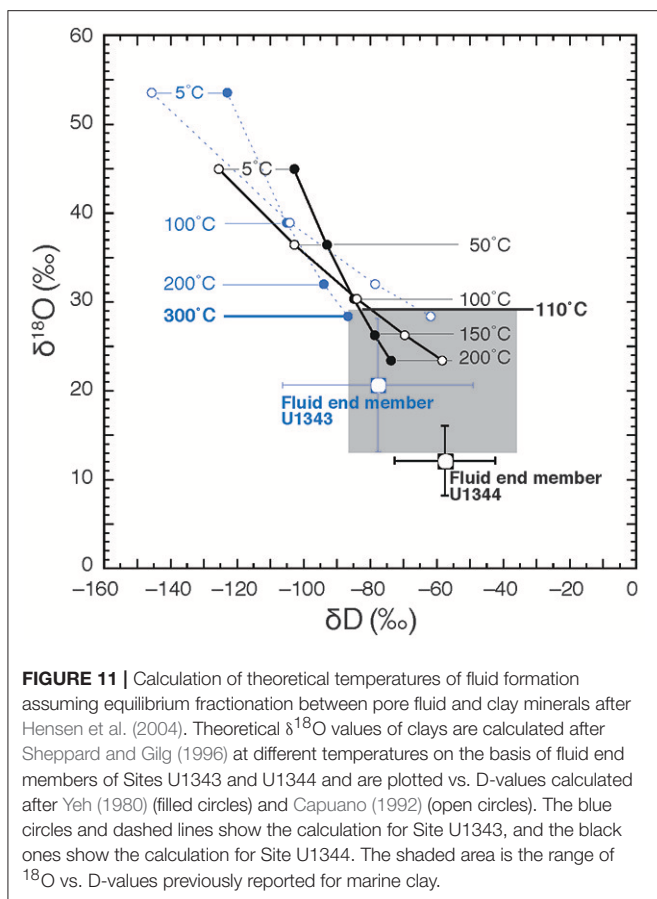


**FIGURE 11 |** Calculation of theoretical temperatures of fluid formation assuming equilibrium fractionation between pore fluid and clay minerals after Hensen et al. (2004). Theoretical  $\delta^{18}\text{O}$  values of clays are calculated after Sheppard and Gilg (1996) at different temperatures on the basis of fluid end members of Sites U1343 and U1344 and are plotted vs. D-values calculated after Yeh (1980) (filled circles) and Capuano (1992) (open circles). The blue circles and dashed lines show the calculation for Site U1343, and the black ones show the calculation for Site U1344. The shaded area is the range of  $^{18}\text{O}$  vs. D-values previously reported for marine clay.

U1343 and U1344 ( $49.0^\circ\text{C km}^{-1}$  and  $53.3^\circ\text{C km}^{-1}$ , respectively; Takahashi et al., 2011b) are linear throughout the cored sediment columns, then the estimated formation temperatures of  $300^\circ\text{C}$  at Site U1343 and  $110^\circ\text{C}$  at Site U1344 correspond to  $\sim 6$  and  $2$  km below the seafloor, respectively.

Isotopic profiles showing  $^{18}\text{O}$  enrichment and D depletion in proportion to  $\text{Cl}^-$  depletion have previously been reported only from active subduction zones and submarine mud volcanoes, settings in which deep-sourced fluids have migrated from several kilometers below the seafloor at temperatures above  $60^\circ\text{C}$  (e.g., Kastner et al., 1993; Dählmann and De Lange, 2003; Hensen et al., 2004). Given the passive continental margin setting of the Bering Sea Slope, advection of deep-sourced fluids is unlikely. Furthermore, the well-defined peaks in isotopic ratios in porewater at 30–50 mbsf, which represents relict bottom water from the last glacial maximum, suggest that upward advection is exceedingly slow at these sites ( $<0.1 \text{ mm y}^{-1}$ ) (Schrag and DePaolo, 1993). Therefore, isotopic disequilibrium between freshwater derived from *in situ* clay mineral dehydration and clay minerals may be more likely at Sites U1343 and U1344.

Under the assumption that the trend showing  $^{18}\text{O}$  enrichment and D depletion in proportion to  $\text{Cl}^-$  depletion was derived from *in situ* clay mineral dehydration such as S-I transformation, we can estimate the amount of newly formed illite during the S-I transformation from the dilution factor. The maximum

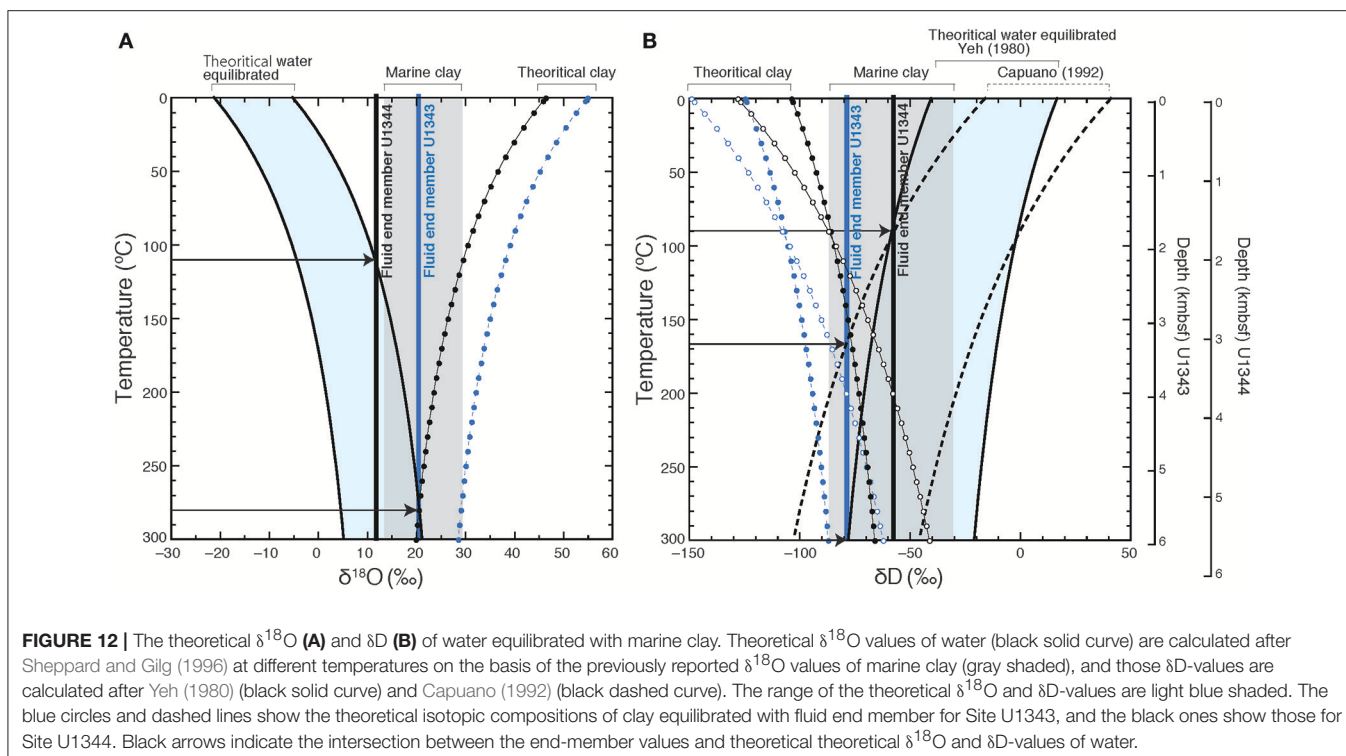
depletion of  $\text{Cl}^-$  was from  $\sim 530 \text{ mM}$  at 130 mbsf to  $\sim 500 \text{ mM}$  at the core bottom (5.7%) at Site U1343 (Figure 2A), and from  $\sim 545 \text{ mM}$  at 140 mbsf to  $\sim 480 \text{ mM}$  at 760 mbsf (12%) at Site U1344 (Figure 2B). At Site U1343, to produce the maximum depletion of porewater  $\text{Cl}^-$  (5.7%) in sediment with a porosity of 55% (the average porosity below 130 mbsf at Site U1343, Figure S8, Takahashi et al., 2011b) requires the production of  $0.031 \text{ g}$  of water per cubic centimeter of sediment. Smectite in marine sediments has been found to bind 17.7–27 wt.% of water (Saffer and Tobin, 2011; Hüpers and Kopf, 2012), depending on environmental conditions. If the bound water value for smectite is assumed to be 20%, then it would take  $0.16 \text{ g}$  smectite/ $\text{cm}^3$  sediment to produce  $0.031 \text{ g}$  water/ $\text{cm}^3$  sediment;  $0.16 \text{ g}$  smectite/ $\text{cm}^3$  amounts to 13 wt.% smectite when dry bulk density is  $1.2 \text{ g}/\text{cm}^3$  (the average value below 130 mbsf at Site U1343, Takahashi et al., 2011b). In other words, 13 wt.% smectite would be transformed to illite under these conditions. Using the same calculation, we estimated 31 wt.% smectite to have been transformed to illite at Site U1344.

### Clay Mineralogy on the Bering Sea Slope

The large proportion of clay-sized particles in the bulk sediment and the high peak intensities of clay minerals in the X-ray diffractograms at Sites U1343 and U1344, compared to those at Site U1341 (Figures 6, 8A), clearly reflect the contrast between the siliciclastic sediments of the Bering Sea Slope (siliciclastics) and the diatom ooze of Bowers Ridge (diatom ooze) (Takahashi et al., 2011a). The high Al contents in the clay-size fractions at Site U1343 and U1344 compared to the contents at Site U1341 (Figure S6), indicating a larger proportion of aluminosilicate in the Bering Sea Slope sediments than at the Bowers Ridge sediments, corroborate this finding. The CIA value of 74 on average at Sites U1343 and U1344 is consistent with the large proportion of clay minerals (Nesbitt and Young, 1982). The constant CIA value with depth suggests that the alteration with burial is too small to be detected. The relatively low CIA value at Site U1341 compared to those from Sites U1343 and U1344 is probably caused by low Al contents, indicating small abundance of aluminosilicate.

Our semi-quantitative estimate that the clay-size fraction in Bering Sea Slope sediment consists of 15–51% smectite, 35–56% illite, 11–29% chlorite, and 2–10% kaolinite (Figure 8B) is consistent with other published clay composition data. Kim et al. (2015) reported that the clay minerals deposited at Site U1343 originated mainly from the Aleutians Islands and that the provenance of clay minerals was not strongly affected by glacial-interglacial environment changes, but some clay mineral compositions during the glacial period after the Mid-Pleistocene Transition (MPT; 200–365 mbsf at Site U1343) showed low illite and relatively high smectite concentrations. They inferred that some sediment from the glacial shelf off Alaska or from glacial rivers in southwestern Alaska may have been transported to Site U1343 during the post-MPT glacial period (Kim et al., 2015). We concur that the clay minerals on the Bering Sea Slope are of mostly detrital origin.

It is difficult to separate the effects of diagenesis from the effects of changing detrital provenance in a clay-rich sediment composed of smectite, illite, and chlorite, even when



the porewater chemistry indicates the occurrence of the S-I transformation. On the basis of observed decrease of  $\text{Cl}^-$  in porewater, we estimated that 13 and 31 wt.% of smectite in the bulk sediment at Sites U1343 and U1344, respectively, was transformed to illite. However, the illite contents in the clay-size fraction (35–56%) as well as the estimated clay-size fraction in the bulk sediment ranges (5–25%) showed large variation. Furthermore, the estimated clay-size fraction in the bulk sediment, separated by centrifuge, may be underestimated because a centrifuge cannot separate all of the clay-size fraction from the sediment. Given that that the previously reported clay-size fraction ( $<4\ \mu\text{m}$ ) ranged from 5 to 48% (25% on average, Aiello and Ravelo, 2012), the maximum increase of 31 wt.% illite would be too small to detect among illite contents in the dry bulk sediments.

### I/S Mixed Layer

The composite reflection of illite-(002)/smectite-(003) at  $2\theta \approx 16^\circ$  in the X-ray diffractograms (Figures 5, 6) documents the presence of the I/S mixed layer (Moore and Reynolds, 1997), which is an indicator of diagenetic S-I transformation (e.g., Hower et al., 1976; Pytte and Reynolds, 1989). The increase of illite content in the I/S mixed layer with increasing depth down to  $\sim 150$  mbsf (Figure 7) may support our inference that I/S formed *in situ* at the Bering Sea Slope sites, at least at depths shallower than 150 mbsf. The relatively high illite contents below  $\sim 150$  mbsf compared to those in shallower areas also imply the occurrence of S-I transformation in the deeper depths. However, most detrital smectite is not pure; rather, it is mixed-layer I/S. For example, in previously well-studied Gulf Coast sediments,

the initial composition of the clay minerals showed roughly 15–20% illite in mixed-layer I/S clay before the start of illitization at around 1000 mbsf, where the temperature is  $60^\circ\text{C}$  (e.g., Hower et al., 1976; Freed and Peacor, 1989). The observed illite contents in the I/S mixed layer ranged from 2 to 17% in our samples, which is generally lower than previously reported values for the initial state before the start of S-I transformation. Therefore, the generally low content and the slight increase of illite contents in the I/S mixed layer observed at Sites U1343 and U1344 are insufficient evidences for *in situ* S-I transformation.

To study the structure of the I/S mixed layer, we examined two clay-mineral-rich samples from Site U1343 under the TEM. Although little S-I transformation was expected from the XRD analysis, we were able to identify one smectite particle  $0.25\ \mu\text{m}$  long containing interlayered illite (Figures 9a,b). Because the small smectite particle was very sensitive to electron beam irradiation, the lattice fringe readily disappeared as a result of amorphization during the TEM observation. We were unable to obtain electron diffraction spots from the I/S mixed layer because of its small amount in the smectite particles. A high-resolution TEM lattice fringe image of the small clay particle showed wavy smectite layers, a structure indicating a low degree of crystallinity that may reflect variability in the chemical composition. A change in interlayer spacing from 1.3 nm to 1.0 nm, identified as the (001) spacing of illite (e.g., Drits et al., 1997), was found within the smectite particle. Such a lateral change of basal spacing within a continuous layer is characteristic of layer-by-layer S-I transformation (Bauluz et al., 2000). Energy-dispersive X-ray analysis showed that these layers at the tip of the smectite particle had higher Al and K contents and lower Mg contents than the

layers in the central part of the particle (**Figure 9c**). This finding is consistent with illite formation, in which Si and Mg are lost and Al and K are gained (Dong et al., 1997).

If the small smectite particle was authigenic smectite formed in the sediment, illite formation in the particle should be a good evidence of *in situ* S-I transformation. However, the authigenic smectite can be reliably identified only if the smectite grown on surfaces or in pore space of glass shards (Masuda et al., 1996). Although the wavy structure of lattice fringes may imply the crystallization occurred at low temperatures and relatively rapid (Masuda et al., 1996), the structure is not sufficient evidence of the *in situ* formation of smectite. Therefore, we cannot say whether the smectite was authigenic.

In summary, the illite contents in the I/S mixed layer determined by XRD as well as the structure of the I/S mixed layer observed by TEM do not provide definitive evidence for *in situ* S-I transformation. Further studies are needed to prove the S-I transformation based on clay mineralogy.

### Fe(III) Reduction in Clay Minerals Below the Sulfate-Methane Transition Zone

At Sites U1343 and U1344, the release of  $\text{Fe}^{2+}$  through S-I transformation promoted by microbial Fe(III) reduction has previously been hypothesized on the basis of precipitation of Fe-rich authigenic carbonate minerals, and relatively high concentrations of dissolved Fe ( $\text{Fe}^{2+}$ ) in porewater (Takahashi et al., 2011b; Pierre et al., 2016). The dissolved Fe concentration reached a maximum of  $60\ \mu\text{M}$  at  $\sim 50$  mbsf at Site 1343 and  $80\ \mu\text{M}$  at  $\sim 150$  mbsf at Site U1344, and Fe concentrations remained appreciable ( $\sim 10$ – $20\ \mu\text{M}$ ) below these depths (**Figures 2G,H**). The decrease of Fe concentrations below  $\sim 50$  mbsf and  $\sim 150$  mbsf at Sites U1343 and U1344 could be attributed to the precipitation of Fe-rich authigenic carbonate (Pierre et al., 2016).

Interestingly, elevated dissolved Fe concentrations were observed below the sulfate methane transition zone (SMTZ) at around  $\sim 8$  mbsf at Sites U1343 and U1344 (Wehrmann et al., 2011), where both methanogenesis and sulfate reduction in association with methane oxidation occurred. According to the classic reduction scheme in marine sediment based on theoretical calculations of energy yields, iron reduction has been thought to be limited to anoxic sediments above the SMTZ and only methanogenesis is thought to occur below the SMTZ (e.g., Berner, 1981; Emerson and Hedges, 2006). A more recent study, however, has indicated that microbial Fe reduction of iron minerals in the methanogenesis zone below the SMTZ and the release of  $\text{Fe}^{2+}$  into porewater are possible (Oni et al., 2015). Indeed, the dissolved Fe concentrations in porewater below the SMTZ at Sites U1343 and U1344 imply that dissimilatory iron reduction occurs below the SMTZ. Recent studies have suggested the novel process of anaerobic oxidation of methane coupled to reduction of Fe (oxyhydr) oxides also releases dissolved Fe ( $\text{Fe}^{2+}$ ) below SMTZs (e.g., Riedinger et al., 2014; Egger et al., 2017). In this case, Fe(III) in clay minerals would not be the major electron acceptor. In addition, the release of  $\text{Fe}^{2+}$  into porewater is not definitive evidence for microbial iron reduction because abiotic

reactions of monosulfides with hydrogen ions also produce free  $\text{Fe}^{2+}$  (Wilkin and Barnes, 1996; Holmkvist et al., 2011).

In this context, our results from  $^{57}\text{Fe}$  Mössbauer spectroscopy of the clay-size fraction clearly show a decrease of  $\text{Fe}^{3+}$  content from 70% of the total Fe in the clay-size fraction near the seafloor to 50% at  $\sim 400$  mbsf. This finding strongly suggests the reduction of Fe(III) in clay minerals occurs below the SMTZ. The decrease of  $\text{Fe}^{3+}$  with depth would not arise from a change in detrital provenance but instead would reflect burial diagenesis, because no corresponding change in clay mineralogy has been observed in the high-resolution record of clay composition at Site U1343 (Kim et al., 2015). In particular, the contents of chlorite, which may contain high concentrations of  $\text{Fe}^{2+}$  (Kalinenko, 2001), does not increase with depth (**Figure 8B**), suggesting no relationship between the change in detrital provenance and the vertical profiles of  $\text{Fe}^{2+}$  contents in the clay fraction. Note that the precipitation of Fe(III) hydroxide from dissolved Fe during core drying should not affect the results of the Mössbauer analysis, because the maximum dissolved Fe concentration in porewater was too small to affect the Fe in the clay fraction. The maximum dissolved Fe concentration was  $80\ \mu\text{M}$  at Site U1344, which amounts to 0.00014 wt.% in bulk sediments when the porosity is 35% and dry bulk density is  $1.1\ \text{g}/\text{cm}^3$  (the average values at Site 1343, Takahashi et al., 2011b). In contrast, the Fe content in the clay-size fraction at Sites U1343 and U1344 ranges from 3.5 to 8.4 wt.% and the clay-size fraction in bulk sediment ranges from 0.3 to 24 wt.% (Table S1), indicating that the minimum Fe content in the bulk sediment is 1.1 wt.%. Therefore, the precipitation of Fe(III) hydroxide during core sample drying should be negligible.

The extent of Fe(III) reduction in the clay-size fraction from the surface to  $\sim 400$  mbsf at the Bering Sea Slope sites (29%) is a reasonable value for microbial Fe(III) reduction in clay because it lies within the range of structural Fe(III) reduction in clay minerals (8–46%) estimated in a culturing study (Kostka et al., 1999). We cannot identify which clay mineral contributed to the reduction of Fe(III) from the Mössbauer spectroscopic analysis of the bulk clay-size fraction. However, experimental results showing that the Fe(III) in chlorite and smectite is more susceptible to microbial reduction than the Fe(III) in illite (Bishop et al., 2011; Zhang et al., 2012) suggest that chlorite and smectite are the main sources. The predominance of smectite over chlorite in the clay-size fraction of Bering Sea Slope sediment implies that smectite accounts for the reduction of Fe(III).

Because both biotic and abiotic iron reduction in smectite has been presumed to be a general phenomenon that accompanies and contributes to S-I transformation (Eslinger et al., 1979; Kim et al., 2004), our results indicate that the potential ability of the clay mineral in Bering Sea Slope sediments to promote S-I transformation.

### Implication for the S-I Transformation at Low Temperature Promoted by the Reduction of Fe(III) in Clay Mineral

Our porewater data strongly suggest the occurrence of the S-I transformation at temperatures below  $40^\circ\text{C}$  in sediment

from the Bering Sea slope. Note that the observed depletion of  $\text{Cl}^-$  (maximum 12%) from seawater value by clay mineral dehydration is smaller than the previously reported values (>20%) from active subduction zones and submarine mud volcanoes (e.g., Kastner et al., 1993; Dählmann and De Lange, 2003; Hensen et al., 2004). The slight depletion of  $\text{Cl}^-$  indicates a little S-I transformation. Indeed, the only slight increase of the illite contents in the I/S mixed layer with depth down to ~150 mbsf was observed at Sites U1343 and U1344. So far, the high resolution data for  $\delta^{18}\text{O}$  and  $\delta\text{D}$  of porewater down to several 100 m below seafloor has been rarely reported. Even if the S-I transformation at low temperature occurred in various places, it would be difficult to be detected without the high resolution isotopic porewater data. On the other hand, the decrease of  $\text{Fe}^{3+}/\text{Fe}^{2+}$  in the clay-size fraction with increasing depth strongly suggests microbial reduction of Fe(III) in clay minerals with burial. Although there is no direct evidence, we speculate that this microbial reduction of Fe(III) contributes the low-temperature S-I transformation in Bering Sea Slope sediment. In contrast, no signs of the S-I transformation were observed at Site U1341 on Bowers Ridge. The difference between Bering Sea Slope and Bowers Ridge sediments should reflect those of their sedimentary environments. The on-board geochemical data obtained during IODP Expedition 323 showed that the concentrations of microbial respiration products such as dissolved inorganic carbon (DIC), ammonium, and phosphate ions in porewater are an order of magnitude higher at Bering Sea Slope sites than at Bowers Ridge site (Takahashi et al., 2011a). This suggests that microbial activity reflects different sedimentation rates of photosynthetic products in the respective water columns (Kallmeyer et al., 2012). As a result, SMTZs at Sites U1343 and U1344 were observed in shallow depths around ~8 mbsf (Wehrmann et al., 2011), and sulfate is present at all depths at U1341 (Wehrmann et al., 2013). Under the availability of sulfate which is a usual reducing agent (electron acceptors) in marine sediments, unusual electron acceptors such as Fe(III) in clay minerals may not be used for redox reaction. Thus, the reduction of Fe(III) in clay minerals may occur only below SMTZ underlying the high-productivity surface seawater. Our results imply the significant ecological roles on the diagenesis of siliciclastic clay minerals underlying the high-productivity surface seawater at continental margins.

## CONCLUSIONS

1) We determined the origin of the freshwater components that dilute the original porewater by using  $\delta^{18}\text{O}$  and  $\delta\text{D}$  data. Plots of  $\text{Cl}^-$  concentrations vs.  $\delta^{18}\text{O}$  and  $\delta\text{D}$  below 120–140 mbsf at Sites U1343 and U1344 indicate that the freshwater components have two origins. The simultaneous enrichment of  $^{18}\text{O}$  and depletion of D in proportion to the depletion of  $\text{Cl}^-$  in porewater with increasing depth strongly suggests the occurrence of the S-I transformation at temperatures below 40°C in sediment from the Bering Sea slope. On the other

hand, the discrete low  $\text{Cl}^-$  spikes observed between ~200 mbsf and ~420 mbsf at Sites U1343 and U1344 could be attributed to the dissociation of methane hydrate.

- 2) We looked for evidence for *in situ* S-I transformation by using XRD analyses and TEM observations of the clay fraction. Although a smectite particle containing interlayered illite was observed, and the illite content in the I/S mixed layer increased with depth down to ~150 mbsf, implying *in situ* S-I transformation, this finding is not sufficiently strong evidence because of the difficulty of discriminating between authigenic and terrestrial I/S mixed layers.
- 3) We evaluated the possibility of a reduction of Fe(III) in clay minerals by  $^{57}\text{Fe}$  Mössbauer spectroscopy of the clay fraction. The decrease of  $\text{Fe}^{3+}$  content in total Fe with increasing depth in conjunction with elevated levels of dissolved Fe in porewater strongly suggest microbial reduction of Fe(III) in clay minerals below the SMTZ, which in turn could promote the S-I transformation.

In conclusion, our results suggest that the low-temperature S-I transformation is mediated by reduction of Fe(III) in clay mineral below SMTZ in the Bering Sea Slope sediment underlying the high-productivity surface seawater.

## AUTHOR CONTRIBUTIONS

AI: proposed the topic and conceived and designed the study; NT carried out the TEM analyses; SW analyzed the major elements in the clay-size fraction; HM helped in the interpretation of XRD analyses and TEM observations; KS and MoM carried out the  $^{57}\text{Fe}$  Mössbauer Spectroscopy; SK and B-KK carried out the XRD analyses; MaM helped with the oxygen isotope analysis of porewater; FI collaborated with AI to prepare the manuscript. All authors read and approved the final manuscript.

## FUNDING

This work was supported in part by JSPS Grant-in-Aid for Scientific Research (17H01871 to AI) and by the Atmospheric Sea-At Technology Development Program (Grant No. KMIPA2015-0606 to B-KK).

## ACKNOWLEDGMENTS

This research used samples and data provided by the IODP. We acknowledge the great support of the IODP Expedition 323 shipboard scientists, technicians, and all crews and drillers on the *JOIDES Resolution*. The authors are grateful to A. Imajyo and O. Tadaï for technical assistance. This is a contribution to the Deep Carbon Observatory (DCO).

## SUPPLEMENTARY MATERIAL

The Supplementary Material for this article can be found online at: <https://www.frontiersin.org/articles/10.3389/feart.2018.00036/full#supplementary-material>



## REFERENCES

- Aiello, I. W., and Ravelo, A. C. (2012). Evolution of marine sedimentation in the Bering Sea since the Pliocene. *Geosphere* 8, 1231–1253. doi: 10.1130/GES00710.1
- Asahi, H., Kender, S., Ikehara, M., Sakamoto, T., Ravelo, A. C., Alvarez-Carikian, C., et al. (2014). Orbital-scale benthic foraminiferal oxygen isotope stratigraphy at the Bering Slope IODP Exp. 323 Site U1343. *Deep-Sea Res. II* 125–126, 66–83. doi: 10.1016/j.dsr2.2014.01.004
- Banfield, J. E., Jones, B. E., and Veblen, D. R. (1991). An AEM-TEM study of weathering and diagenesis, Abert Lake, Oregon: I. Weathering reactions in the volcanics. *Geochim. Cosmochim. Acta* 55, 2781–2798. doi: 10.1016/0016-7037(91)90444-A
- Bauluz, B., Peacor, D. R., and Lopez, J. M. G. (2000). Transmission electron microscopy study of illitization in pelites from the Iberian Range, Spain: layer-by-layer replacement? *Clays Clay Miner.* 48, 374–384. doi: 10.1346/CCMN.2000.0480308
- Berner, R. A. (1981). A new geochemical classification of sedimentary environments. *J. Sediment Petrol.* 51, 359–365.
- Biscaye, P. E. (1965). Mineralogy and sedimentation of recent deep-sea clay in the Atlantic Ocean and adjacent seas and oceans. *Geol. Soc. Am. Bull.* 76, 803–832. doi: 10.1130/0016-7606(1965)76[803:MASAPD]2.0.CO;2
- Bishop, M. E., Dong, H. L., Kukkadapu, R. K., and Edelman, R. E. (2011). Microbial reduction of Fe(III) in multiple clay minerals by *Shewanella putrefaciens* and reactivity of bioreduced clay minerals toward Tc(VII) immobilization. *Geochim. Cosmochim. Acta* 75, 5229–5246. doi: 10.1016/j.gca.2011.06.034
- Brown, K. M., Saffer, D. M., and Bekins, B. A. (2001). Smectite diagenesis, porewater freshening, and fluid flow at the toe of the Nankai wedge. *Earth Planet. Sci. Lett.* 194, 97–109. doi: 10.1016/S0012-821X(01)00546-5
- Bruce, C. H. (1984). Smectite dehydration: its relation to structural development and hydrocarbon accumulation in northern Gulf of Mexico basin. *AAPG Bull.* 68, 673–683.
- Buatier, M. D., Peacor, D. P., and O'Neil, J. R. (1992). Smectite-illite transition in Barbados accretionary wedge sediments: TEM and AEM evidence for dissolution/crystallization at low temperature. *Clays Clay Miner.* 40, 65–80. doi: 10.1346/CCMN.1992.0400108
- Capuano, R. M. (1992). The temperature dependence of hydrogen isotope fractionation between clay minerals and water: evidence from a geopressed system. *Geochim. Cosmochim. Acta* 56, 2547–2554. doi: 10.1016/0016-7037(92)90208-Z
- Cooper, A. K., Scholl, D. W., and Marlow, M. S. (1987). "Structural framework, sedimentary sequences, and hydrocarbon potential of the Aleutian and Bowers Basins, Bering Sea," in *Geology and Resource Potential of the Continental Margin of Western North America and Adjacent Ocean Basins—Beaufort Sea to Baja California*, Vol. 6, eds D. W. Scholl, A. Grantz, and J. Vedder (Washington, DC: Earth Sci. Ser. Houston Circum-Pacific Council for Energy and Mineral Resources), 476–502.
- Craig, H. (1961). Isotopic variations in meteoric waters. *Science* 133, 1702–1703. doi: 10.1126/science.133.3465.1702
- Dählmann, A., and De Lange, G. J. (2003). Fluid-sediment interactions at eastern Mediterranean mud volcanoes: a stable isotope study from ODP Leg 160. *Earth Planet. Sci. Lett.* 212, 377–391. doi: 10.1016/S0012-821X(03)00227-9
- Dong, H., Peacor, R. D., and Freed, R. L. (1997). Phase relations among smectite, R1 illite-smectite, and illite. *Am. Mineral.* 82, 379–391. doi: 10.2138/am-1997-3-416
- Drits, V., Srodoft, J., and Eberl, D. D. (1997). XRD measurement of mean crystallite thickness of illite and illite/smectite: reappraisal of the Kubler index and the Scherrer equation. *Clays Clay Miner.* 45, 461–475. doi: 10.1346/CCMN.1997.0450315
- Eberl, D., and Hower, J. (1976). Kinetics of illite formation. *Geol. Soc. Am. Bull.* 87, 1326–1330. doi: 10.1130/0016-7606(1976)87<1326:KOIF>2.0.CO;2
- Egger, M., Hagens, M., Sapart, C. J., Dijkstra, N., van Helmond, N. A. G. M., Mogollón, J. M., et al. (2017). Iron oxide reduction in methane-rich deep Baltic Sea sediments. *Geochim. Cosmochim. Acta* 207, 256–276. doi: 10.1016/j.gca.2017.03.019
- Emerson, S., and Hedges, J. (2006). "Sediment diagenesis and benthic flux," in *Treatise on Geochemistry: The Oceans and Marine Geochemistry*, ed H. Elderfield (Oxford: Elsevier), 293–319.
- Eslinger, E., Highsmith, P., Albers, D., and De Mayo, B. (1979). Role of iron reduction in the conversion of smectite to illite in bentonites in the Disturbed Belt, Montana. *Clays Clay Miner.* 27, 327–338. doi: 10.1346/CCMN.1979.0270503
- Freed, R. L., and Peacor, D. R. (1989). Geopressed shale and sealing effect of the smectite to illite transition. *Am. Assoc. Petrol. Geol. Bull.* 73, 1223–1232.
- Guo, J., and Underwood, M. B. (2011). "Data report: refined method for calculating percentages of kaolinite and chlorite from X-ray diffraction data, with application to the Nankai margin of southwest Japan," in *Proc. IODP, 314/315/316*, eds M. Kinoshita, H. Tobin, J. Ashi, G. Kimura, S. Lallemand, E. J. Scream, D. Curewitz, H. Masago, K.T. Moe, and the Expedition 314/315/316 Scientists (Washington, DC: Integrated Ocean Drilling Program Management International, Inc.). doi: 10.2204/iodp.proc.314315316.201.2011
- Hathon, E. G. (1992). *X-Ray Diffraction and Transmission Electron Microscopy Study of the Surface Charge on the Illite and Smectite Components of Illite/Smectite Mixed-Layer Clays*. Ph.D. dissertation, Univ. of Missouri, Columbia.
- Hensen, C., Wallman, K., Schmidt, M., Ranero, C. R., and Suess, E. (2004). Fluid expulsion related to mud extrusion off Costa Rica—A window to the subducting slab. *Geology* 32, 201–204. doi: 10.1130/G20119.1
- Hesse, R., and Harrison, W. E. (1981). Gas hydrates (clathrates) causing pore-water freshening and oxygen isotope fractionation in deep-water sedimentary sections of terrigenous continental margins. *Earth Planet. Sci. Lett.* 55, 453–462. doi: 10.1016/0012-821X(81)90172-2
- Holmkvist, L., Ferdelman, T. G., and Jørgensen, B. B. (2011). A cryptic sulfur cycle driven by iron in the methane zone of marine sediment (Aarhus Bay, Denmark). *Geochim. Cosmochim. Acta* 75, 3581–3599. doi: 10.1016/j.gca.2011.03.033
- Horikawa, K., Martin, E. E., Basak, C., Onodera, J., Seki, O., Sakamoto, T., et al. (2015). Pliocene cooling enhanced by flow of low-salinity Bering Sea water to the Arctic Ocean. *Nat. Commun.* 6:7587 doi: 10.1038/ncomms8587
- Hover, V. C., Walter, L. M., and Peacor, D. R. (2002). K uptake by modern estuarine sediments during early marine Diagenesis, Mississippi Delta Plain, Louisiana, U.S.A. *J. Sediment. Res.* 72, 775–792. doi: 10.1306/032502720775
- Hower, J., Eslinger, E., Hower, M. E., and Perry, E. A. (1976). Mechanism of burial metamorphism of argillaceous sediment: 1. Mineralogical and chemical evidence. *GSA Bull.* 87, 725–737. doi: 10.1130/0016-7606(1976)87<725:MOBMOA>2.0.CO;2
- Huang, W. L., Longo, J. M., and Pevear, D. V. (1993). An experimentally derived kinetic model for smectite-to-illite conversion and its use as a geothermometer. *Clays Clay Miner.* 41, 162–177. doi: 10.1346/CCMN.1993.0410205
- Hüpers, A., and Kopf, A. J. (2012). Effect of smectite dehydration on pore water geochemistry in the shallow subduction zone: an experimental approach. *Geochem. Geophys. Geosyst.* 13:Q0AD26. doi: 10.1029/2012GC004212
- Ijiri, A., Harada, N., Hirota, A., Tsunogai, U., Ogawa, N. O., Itaki, T., et al. (2012). Biogeochemical processes involving acetate in sub-seafloor sediments from the Bering Sea shelf break. *Org. Geochem.* 48, 47–55. doi: 10.1016/j.orggeochem.2012.04.004
- Inoue, A., Velde, B., Meunier, A., and Touchard, G. (1988). Mechanism of illite formation during smectite-to-illite conversion in a hydrothermal system. *Am. Mineral.* 73, 1325–1334.
- Kalinenko, V. V. (2001). Clay minerals in sediments of the Arctic Seas. *Lithol. Miner. Resour.* 36, 362–372. doi: 10.1023/A:1010414305264
- Kallmeyer, J., Pockalny, R., Adhikari, R., Smith, D., and D'Hondt, S. (2012). Global distribution of microbial abundance and biomass in subseafloor sediment. *Proc. Natl. Acad. Sci. U.S.A.* 109, 16213–16216. doi: 10.1073/pnas.1203849109
- Kastner, M., Elderfield, H., Jenkins, W. J., Gieskes, J. M., and Gamo, T. (1993). Geochemical and isotopic evidence for fluid flow in the western Nankai subduction zone, Japan. *Proc. Ocean Drill. Program Sci. Results* 131, 397–413.
- Kastner, M., Elderfield, H., and Martin, J. B. (1991). Fluids in convergent margins—What do we know about their composition, origin, role in diagenesis and importance for oceanic chemical fluxes? *Philos. Trans. R. Soc. London Ser. A Math. Phys. Sci.* 335, 243–259. doi: 10.1098/rsta.1991.0045
- Kim, J., Dong, H., Seabaugh, J., Newell, S. W., and Eberl, D. D. (2004). Role of microbes in the smectite-to-illite transformation. *Science* 303, 830–832. doi: 10.1126/science.1093245
- Kim, J. W., Peacor, D. R., Tessier, D., and Elsass, E. (1995). A technique for maintaining texture and permanent expansion of smectite interlayers for TEM observations. *Clays Clay Miner.* 43, 51–57. doi: 10.1346/CCMN.1995.0430106

- Kim, S., Khim, B.-K., and Cho, H. G. (2015). Clay mineral stratigraphy during the last 2.4 Ma at IODP Exp. 323 Site U 1343 in the Bering Sea. *Mar. Geol.* 359, 163–168. doi: 10.1016/j.margeo.2014.10.004
- Koo, T. H., Lee, G., and Kim, J. W. (2016). Biogeochemical dissolution of nontronite by *Shewanella oneidensis* MR-1: Evidence of biotic illite formation. *Appl. Clay Sci.* 134, 13–18. doi: 10.1016/j.clay.2016.03.030
- Kostka, J. E., Wu, J., Neelson, K. H., and Stucki, J. W. (1999). The impact of structural Fe(III) reduction by bacteria on the surface chemistry of smectite clay minerals. *Geochim. Cosmochim. Acta* 63, 3705–3713. doi: 10.1016/S0016-7037(99)00199-4
- Lynch, F. L., Mack, L. E., and Land, L. S. (1997). Burial diagenesis of illite/smectite in shales and the origins of authigenic quartz and secondary porosity in sandstones. *Geochim. Cosmochim. Acta* 66, 439–446. doi: 10.1016/S0016-7037(97)00066-5
- Maekawa, T. (2004). Experimental study on isotopic fractionation in water during gas hydrate formation. *Geochem. J.* 38, 129–138. doi: 10.2343/geochemj.38.129
- Manheim, F. T., and Sayles, F. L. (1974). "Composition and origin of interstitial waters of marine sediments, based on deep sea drill cores," in *Marine Chemistry, The Sea, Vol. 5*. ed E. D. Goldberg (New York, NY: Wiley-Interscience), 527–568.
- Masuda, H., O'Neil, J. R., Jiang, W.-T., and Peacor, D. R. (1996). Relation among interlayer composition of diagenetic smectite, mineral assemblages, I/S reaction rates, and fluid composition in silicic ash of the Nankai Trough. *Clays Clay Miner.* 44, 443–459.
- Moore, D. M., and Reynolds, R. C. Jr. (1997). *X-ray Diffraction and the Identification and Analysis of Clay Minerals, 2nd Edn.* New York, NY: Oxford University Press.
- Nesbitt, H. W., and Young, G. M. (1982). Early Proterozoic climates and plate motions inferred from major element chemistry of lutites. *Nature* 299, 715–717. doi: 10.1038/299715a0
- Okazaki, Y., Ulincy, A. J., Alvarez Zarkian, C. A., and Asahi, H. (2016). "Data report: benthic foraminiferal stable isotope records at Site U1344, Integrated Ocean Drilling Program Expedition 323," in *Proceedings of the Integrated Ocean Drilling Program Vol. 323*, eds K. Takahashi, A. C. Ravelo, C. A. Alvarez Zarkian, and the Expedition 323 Scientists (Tokyo: Integrated Ocean Drilling Program Management International, Inc.). doi: 10.2204/iodp.proc.323.203.2016
- Oni, O., Miyatake, T., Kasten, S., Richter-Heitmann, T., Fischer, D., Wagenknecht, L., et al. (2015). Distinct microbial populations are tightly linked to the profile of dissolved iron in the methanic sediments of the Helgoland mud area. *North Sea. Front. Microbiol.* 6:365. doi: 10.3389/fmicb.2015.00365
- Perry, E. A., and Hower, J. (1972). Late-stage dehydration in deeply buried pelitic sediments. *AAPG Bull.* 56, 2013–2021.
- Perry, E., and Hower, J. (1970). Burial diagenesis in Gulf Coast pelitic sediments. *Clays Clay Miner.* 18, 167–177. doi: 10.1346/CCMN.1970.0180306
- Pierre, C., Blanc-Valleron, M.-M., Caqueneau, S., März, C., Ravelo, A. C., Takahashi, K., et al. (2016). Mineralogical, geochemical and isotopic characterization of authigenic carbonates from the methane-bearing sediments of the Bering Sea continental margin (IODP Expedition 323, Sites U1343–U1345). *Deep-Sea Res. Pt. II* 125–126, 133–144. doi: 10.1016/j.dsr2.2014.03.011
- Pytte, A. M., and Reynolds, R. C. (1989). "The thermal transformation of smectite to illite," in *McCulloh Thermal History of Sedimentary Basins* eds N. D. Naeser and T. H. McCulloh (Berlin: Springer-Verlag), 133–140.
- Riedinger, N., Formolo, M. J., Lyons, T. W., Henkel, S., Beck, A., and Kasten, S. (2014). An inorganic geochemical argument for coupled anaerobic oxidation of methane and iron reduction in marine sediments. *Geobiology* 12, 172–181. doi: 10.1111/gbi.12077
- Saffer, D. M., and Tobin, H. J. (2011). Hydrogeology and mechanics of subduction zone forearcs: fluid flow and pore pressure. *Annu. Rev. Earth Planet. Sci.* 39, 157–186. doi: 10.1146/annurev-earth-040610-133408
- Savin, S. M., and Epstein, S. (1970). The oxygen and hydrogen isotope geochemistry of clay minerals. *Geochim. Cosmochim. Acta* 34, 25–42. doi: 10.1016/0016-7037(70)90149-3
- Schrag, D. P., and DePaolo, D. J. (1993). Determination of  $\delta^{18}\text{O}$  of seawater in the deep ocean during the last glacial maximum. *Paleoceanography* 8, 1–6. doi: 10.1029/92PA02796
- Sheppard, S. M. F., and Gilg, H. A. (1996). Stable isotope geochemistry of clay minerals. *Clay Miner.* 31, 1–24. doi: 10.1180/claymin.1996.031.1.01
- Springer, A. M., McRoy, C. P., and Flint, M. V. (1996). The Bering Sea Green Belt: shelf-edge processes and ecosystem production. *Fish Oceanogr.* 5, 205–223. doi: 10.1111/j.1365-2419.1996.tb00118.x
- Suchecky, R. K., and Land, L. S. (1983). Isotopic geochemistry of burial-metamorphosed volcanogenic sediments, great valley sequence, Northern California. *Geochim. Cosmochim. Acta* 47, 1487–1499. doi: 10.1016/0016-7037(83)90308-3
- Takahashi, K., Ravelo, A. C., Zarkian, C. A., and the IODP Expedition, 323 Scientists (2011a). IODP Expedition 323 Pliocene and Pleistocene paleoceanographic changes in the Bering Sea. *Sci. Drill.* 11, 4–13. doi: 10.5194/sd-11-4-2011
- Takahashi, K., Ravelo, A. C., Zarkian, C. A., and the Expedition 323 Scientists. (2011b). *Proceedings of the Integrated Ocean Drilling Program 323*. Tokyo: Integrated Ocean Drilling Program Management International, Inc.
- Uramoto, G., Morono, Y., Uematsu, K., and Inagaki, F. (2014). An improved sample preparation method for imaging microstructures of fine-grained marine sediment using microfocus X-ray computed tomography and scanning electron microscopy. *Limnol. Oceanogr. Methods* 12, 469–483. doi: 10.4319/lom.2014.12.469
- Ussler, W. I. I., and Paull, C. K. (2001). "Ion exclusion associated with marine gas hydrate deposits," in *Natural Gas Hydrates: Occurrence, Distribution, and Detection, Vol. 24, Geophysical Monograph*, eds C. K. Paull, and W. P. Dillon (New York, NY: Wiley), 41–51.
- Wehrmann, L. M., Arndt, S., März, C., Ferdelman, T. G., and Brunner, B. (2013). The evolution of early diagenetic signals in Bering Sea subseafloor sediments in response to varying organic carbon deposition over the last 4.3 Ma. *Geochim. Cosmochim. Acta* 109, 175–196. doi: 10.1016/j.gca.2013.01.025
- Wehrmann, L. M., Risgaard-Petersen, N., Schrum, H. N., Walsh, E. A., Huh, Y., Ikehara, M., et al. (2011). Coupled organic and inorganic carbon cycling in the deep subseafloor sediment of the northeastern Bering Sea Slope (IODP Exp. 323). *Chem. Geol.* 284, 251–261. doi: 10.1016/j.chemgeo.2011.03.002
- Whitney, G. (1990). Role of water in the smectite-to-illite reaction. *Clays Clay Miner.* 38, 343–350. doi: 10.1346/CCMN.1990.0380402
- Whitney, G., and Northrop, H. R. (1988). Experimental investigation of the smectite to illite reaction: dual reaction mechanisms and oxygen-isotope systematics. *Am. Mineral.* 73, 77–90.
- Wilkin, R. T., and Barnes, H. L. (1996). Pyrite formation by reactions of iron monosulfides with dissolved inorganic and organic sulfur species. *Geochim. Cosmochim. Acta* 60, 4167–4179. doi: 10.1016/S0016-7037(97)81466-4
- Yeh, H. W. (1980). D/H ratios and late-stage dehydration of shales during burial. *Geochim. Cosmochim. Acta* 44, 341–352. doi: 10.1016/0016-7037(80)90142-8
- Zhang, G., Dong, H., Kim, J. W., and Eberl, D. D. (2007a). Microbial reduction of structural  $\text{Fe}^{3+}$  in nontronite by a thermophilic bacterium and its role in promoting the smectite to illite reaction. *Am. Mineral.* 92, 1411–1419. doi: 10.2138/am.2007.2498
- Zhang, G., Kim, J. W., Dong, H., and Sommer, A. J. (2007b). Microbial effects in promoting the smectite to illite reaction: role of organic matter intercalated in the interlayer. *Am. Mineral.* 92, 1401–1410. doi: 10.2138/am.2007.2331
- Zhang, J., Dong, H., Liu, D., Fischer, T. B., Wang, S., and Huang, L. (2012). Microbial reduction of Fe(III) in illite-smectite minerals by methanogen *Methanosarcina mazei*. *Chem. Geol.* 292–293, 35–44. doi: 10.1016/j.chemgeo.2011.11.003

**Conflict of Interest Statement:** The authors declare that the research was conducted in the absence of any commercial or financial relationships that could be construed as a potential conflict of interest.

Copyright © 2018 Ijiri, Tomioka, Wakaki, Masuda, Shozugawa, Kim, Khim, Murayama, Matsuo and Inagaki. This is an open-access article distributed under the terms of the Creative Commons Attribution License (CC BY). The use, distribution or reproduction in other forums is permitted, provided the original author(s) and the copyright owner are credited and that the original publication in this journal is cited, in accordance with accepted academic practice. No use, distribution or reproduction is permitted which does not comply with these terms.